

UNIVERSITY OF TARTU
Faculty of Science and Technology
Institute of Technology

Sander Suurpere

**DESIGN AND IMPLEMENTATION OF A COSMIC RAY MUON
DETECTOR**

Master's thesis (30 ECTS)
Robotics and Computer Engineering

Supervisors:
Madis Kiisk, PhD
Anzori Georgadze, PhD

Tartu 2019

Design and Implementation of a Cosmic Ray Muon Detector

Abstract

Research in the recent two decades has proven detection devices based on cosmic ray muons to be a viable safe alternative to detection technologies using artificial ionizing radiation. Furthermore, some scientific groups have proved the use of other cosmic ray particles in combination with muons to be usable in the detection of illicit materials other than special nuclear materials (SNM).

The thesis gives an overview of some of the methods that are used to detect cosmic ray muons and exploit them for practical applications. Additionally, the thesis describes the various steps that have to be taken to build a miniature scintillating detection plate. As a part of an ongoing project a single detection plate consisting of 256 fibres was designed along with several mechanical details needed for it to be functional.

The experimental part consisted of constructing a real detector with an active scintillating area of approximately 70mmx70mm that is in principle capable of separating the hit location of a charged particle. The resulting work also highlighted many practical issues that usually cannot be found from literature.

Keywords: particle, detector, scintillator, fibre, muography, tomography, muon

CERCS: T110 Instrumentation technology; P211 High energy interactions, cosmic rays

Kosmilise kiirguse müüonitel põhineva detektori disain ja teostus

Lühikokkuvõte

Viimastel aastakümnetel läbi viidud uurimused on tõestanud, et kosmilise kiirguse müüonitel põhinevad tuvastusseadmed võivad saada turvaliseks alternatiiviks kunstlikul ioniseerival kiirgusel põhinevatele tuvastustehnoloogiatele. Peale selle on mõned teadusgrupid näidanud, et rakendades lisaks müüonitele ka teisi kosmilise kiirguse osakesi on peale raskete tuumade võimalik tuvastada ka kergemaid keelatud aineid.

Töö annab ülevaate mõnedest meetoditest, mida kasutatakse kosmilise kiirguse müüonite mõõtmiseks ja nende rakendamiseks praktilistes lahendustes. Lisaks kirjeldab töö väikesemõõtmelise stsintillatsioonidetektori valmimiseks vajalikke samme. Käimasoleva projekti raames disainiti 256-st stsintillatsioonkiust koosnev detektorplaat ning mitmed mehaanilised detailid, mis seadme toimimiseks vajalikud on.

Eksperimentaalne osa koosnes reaalse detektori ehitamisest. Valminud seadme 70mmx70mm efektiivne ala on võimeline eristama laetud osakeste asukohti. Lisaks tõstis eksperimentaalne töö esile mitmeid kirjandusest sageli puuduvaid praktilisi probleeme, mis stsintillatsioonidetektori ehitamisel esile võivad kerkida.

Märksõnad: osake, detektor, stsintillaator, kiud, müograafia, tomograafia, müüon

CERCS: T110 Instrumentatsioonitehnoloogia; P211 Kõrgenergeetiliste vastasmõjude uuringud, kosmiline kiirgus

Contents

List of Figures	6
List of Tables	7
Abbreviations	8
Introduction	9
1 Principles of muon detectors	10
1.1 Muography and muon tomography	10
1.2 Soft cosmic ray tomography	11
1.3 Modern scintillating fibre detectors	11
1.3.1 The Glasgow MT detector	11
1.3.2 LHCb LS2 upgrade	12
2 Detector design	14
2.1 Active area	14
2.2 SiPM arrays and housing	15
2.3 Rules of coincidence	16
2.4 DAQ	18
2.5 Muon telescope	19

3	Experimental progress	21
3.1	Fibres	21
3.2	Assembling the fibre mats	22
3.2.1	Preparing the aligning table	22
3.2.2	Preparing the epoxy	23
3.2.3	Aligning the fibres	24
3.3	Connecting fibres to SiPM arrays	25
3.4	Polishing	25
3.5	The working system	28
3.6	Open issues	29
	Conclusion	31
	Acknowledgements	32
	Bibliography	33
	A Drawings	36
	Lihtlitsents	45

List of Figures

1.1	CAD model depicting the muon tomograph developed in Glasgow	12
1.2	CAD model of a finished LHCb fibre mat module.	13
2.1	Ideal fibre placement	14
2.2	CAD model of a single detector plate.	15
2.3	CAD model of Hamamatsu MPPC® array housing	16
2.4	A schematic view of how fibres are bundled together	17
2.5	DAQ board	19
2.6	Muon telescope	20
3.1	Alignment table	23
3.2	Cross-sectional view of a dummy fibre mat	24
3.3	Post-curing procedures.	25
3.4	Polishing the fibres individually.	26
3.5	Result of the polishing procedure as seen under an optical microscope.	27
3.6	The final polishing method.	27
3.7	Final steps before data acquisition.	28
3.8	Measurements using an UV source	28
3.9	UV source attached to a single fibre.	29

List of Tables

2.1	Individual fibre positions in the left interface.	17
2.2	Individual fibre positions in the right interface.	18

Abbreviations

ASIC – Application-specific integrated circuit

CERN – European Organization for Nuclear Research

LHCb – Large Hadron Collider beauty

MPPC – Multi-Pixel Photon Counter

MT – Muon tomography

PLA – Poly(lactic acid)

PMMA – Poly(methyl 2-methylpropenoate)

PMT – Photomultiplier tube

PS – Poly(1-phenylethene)

SNM – Special nuclear material

SciFi – Scintillating fibre

SiPM – Silicon photomultiplier

VOI – Volume of interest

Introduction

Scanning the insides of a container by non-invasive means traditionally implies the use of an external radiation source, e.g. an X-ray source. Artificial sources of ionizing radiation impose additional safety restrictions, require operating costs and may inflict psychological stress among the population. Alternative methods relying on the existence of background radiation can potentially replace or complement the existing scanning systems in the near future.

A significant number of muographic and tomographic devices relying on cosmic rays have been built in the last two decades [1, 2, 3, 4, 5, 6, 7]. The very first implementation of such a tomographic system was constructed in Los Alamos National Laboratory, the first results being published in 2003 by Borozdin et al. [1]. Various scientific groups have created similar devices that differ in build materials, reconstruction methods and even the types of particles exploited in the design.

Unfortunately, to use such a device for either cosmic ray research or commercially, a fully functional detector cannot simply be bought from the store or ordered online. Although some companies that focus on the production of full size tomographs have emerged [8], using such a device is still in large part dependent on the ability and willingness of the user to build a custom device from scratch.

The thesis is motivated by an ongoing muon tomography project [9, 10] and serves multiple purposes. The main objective is to develop a preliminary detector module that would not only count ionizing particles but also be position sensitive. The second purpose is to act as a first experimental step towards building a muon telescope. Finally, the thesis should also help any future scintillating fibre device builders by describing detector assembly techniques and characterizing the performance parameters.

Chapter 1

Principles of muon detectors

1.1 Muography and muon tomography

Cosmic rays are a type of natural background radiation originating from astrophysical sources. Primary cosmic rays, mostly protons hit the atmosphere and produce a cascade of particles. This stream of particles has a variable composition that is dependent on the vertical distance from ground [11]. The most numerous type of particle at sea level is the muon, the flux of which for a horizontal detector is approximately $1 \text{ cm}^{-2} \text{ min}^{-1}$ [11].

The existing natural flux of cosmic ray muons can be used by measuring the attenuation of the flux in the presence of a very large or dense object. Furthermore, another physical effect called multiple Coulomb scattering can be exploited. An incident muon will change its exiting direction, compared to the incident direction, if it travels through matter. This change is dependent on the atomic number (Z) and thickness (x) of the material, as well as the momentum (p) of the particle. For muons the relationship is often represented by the approximation

$$\theta = \frac{14\text{MeV}}{\beta c p} \sqrt{\frac{x}{X_0}}, \quad (1.1)$$

where βc is the velocity of the particle, p is its momentum in MeV and the radiation length is

$$X_0 = \frac{716.4}{Z(Z+1) \ln \frac{287}{Z}} \frac{\text{g}}{\text{cm}^2}. \quad (1.2)$$

Measuring the change of direction of a particle and applying an appropriate reconstruction algorithm makes it possible to use cosmic ray muons to create 3D tomographic images of a volume of interest (VOI) [12].

1.2 Soft cosmic ray tomography

Designing a tomographic system exclusively on the scattering of muons consequently means that the system is not capable of differentiating low Z materials. This is due to the fact that the mean muon scattering angles do not differ enough across separate low-atomic number materials. In order to design a device that can also detect low Z materials, additional physical effects and/or elementary particles and their properties should be exploited.

In 2015 Blanpied et al. demonstrated the possibility of combining the Coulomb scattering of cosmic ray muons with the scattering of cosmic ray electrons in order to discriminate between medium and light elements [13]. Expanding the range of cosmic ray tomography's usefulness towards low Z material discrimination is crucial, as this enables us to not only discover SNMs, but also explosives, illicit drugs and other problematic substances.

1.3 Modern scintillating fibre detectors

Although there are many ways to construct a particle detector, some of the existing designs have proved to be especially useful for the development of the ongoing project related to this thesis. Below are some of the designs that have had the most influence on the thesis.

1.3.1 The Glasgow MT detector

The Glasgow muon tomograph was built in order to screen legacy nuclear waste in the UK [7]. The project began in 2009 and the first results were published in 2013. The tomograph uses 2mm diameter plastic scintillating fibres in its active area. The fibres are placed into planes consisting of 128 fibres. Placing two planes parallel to each other while keeping the fibres of the two planes orthogonal creates a detection module that reveals both the X- and Y-direction of a passing particle. These detection modules are then stacked on top of each other to determine the scattering angle of a cosmic ray muon.

In order to keep the fibres together the Glasgow researchers made use of Rohacell® support sheets which are made of a low Z material and do not affect the measurements significantly [7].

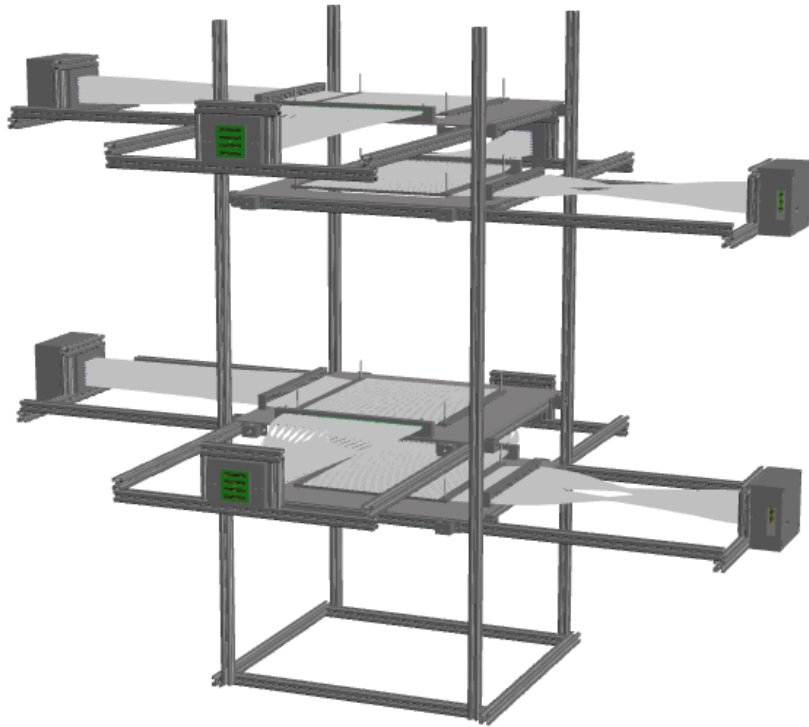


Figure 1.1: CAD model depicting the muon tomograph developed in Glasgow [14].

Their fibres are connected to Hamamatsu PMTs in groups of two and a muon hit is registered by finding the fibre with the strongest signal.

1.3.2 LHCb LS2 upgrade

During the second Long Shutdown (LS2) of the Large Hadron Collider at CERN, the LHCb experiment will undergo an upgrade [15]. One of the changes that will be made is replacing the cylindrical drift tubes of the Outer Tracker with scintillating fibres due to the fact that increasing the luminosity at LHCb multiple times causes the drift time to "spill over" to the next measurement. In other words, the time resolution of the existing tracking system is not good enough for the upgrade.

Although not a cosmic ray experiment, the LHCb happens to be a good example on how to construct SciFi modules. The fibre mats are constructed by winding six layers of 0.25mm fibres over an aluminium wheel containing grooves to align the fibres. The wheel is treated with a sealer, a release agent and the fibres are held together with the help of TiO_2 filled epoxy. After the epoxy is cured, the mat is released from the wheel, inspected and connected to SiPMs.

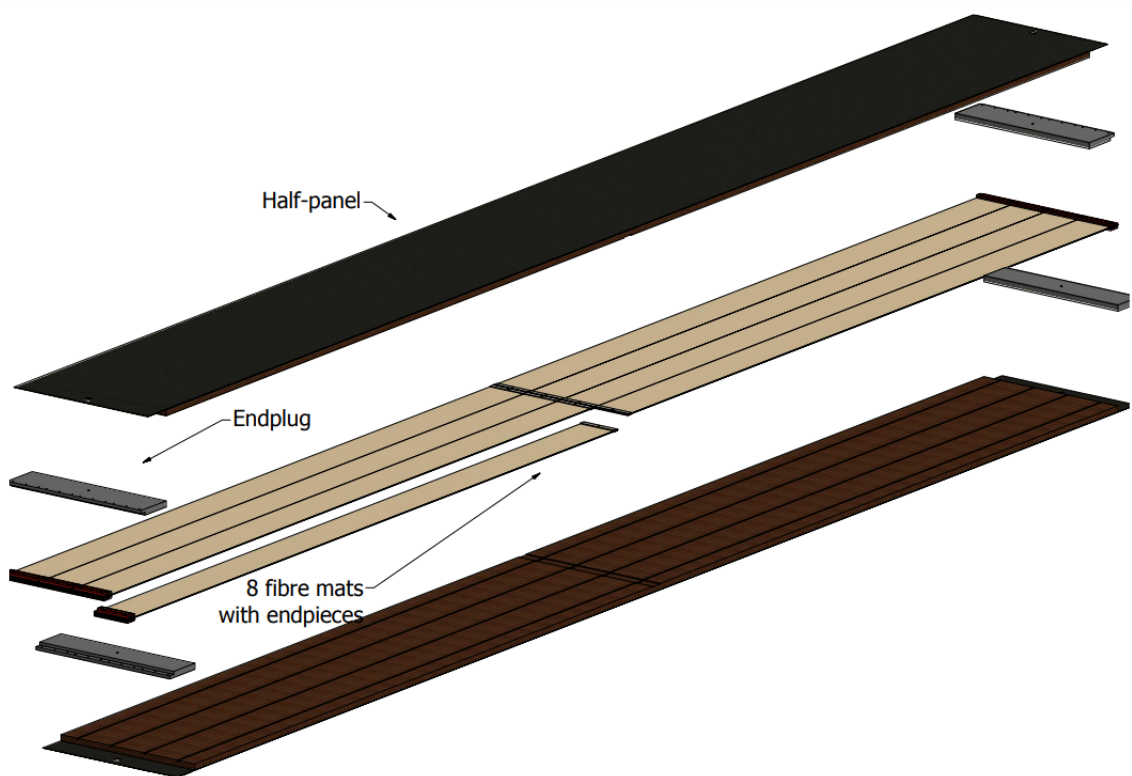


Figure 1.2: CAD model of a finished LHCb fibre mat module [15].

Chapter 2

Detector design

The main components that make up the existing detector as well as a future cosmic ray telescope are scintillating fibre detection plates, SiPM array modules and a DAQ system. Before the system could be assembled, the exact configuration of fibre positioning, mechanical details and coincidence rules had to be designed.

2.1 Active area

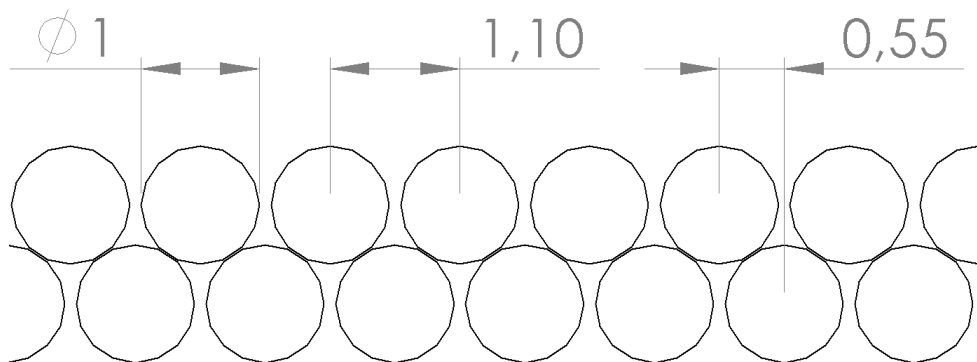
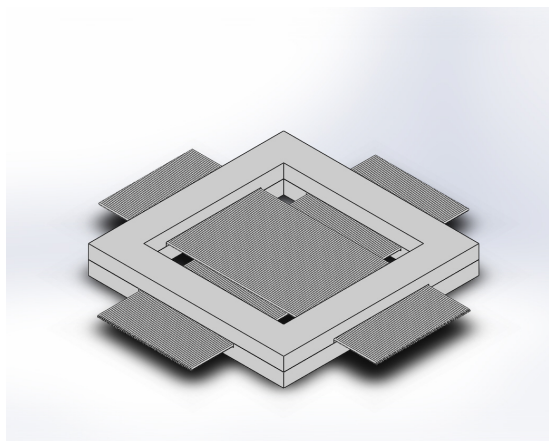
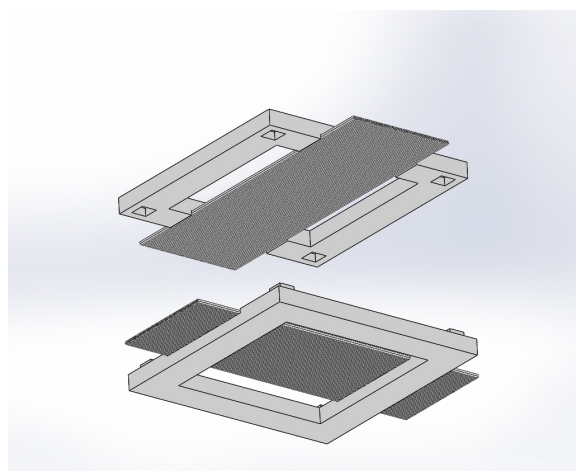


Figure 2.1: Ideal fibre placement in the active area of the detector. Dimensions are expressed in millimeters.

Choosing the building blocks for the active region of a SciFi detector, i.e. the scintillating



(a) Frame assembly with fibres.



(b) Exploded view of the plate model from below.

Figure 2.2: CAD model of a single detector plate.

components, is an interplay between cost, spatial resolution and light yield. Fibres with a round cross-section happen to be considerably less expensive compared to other shapes, thereby allowing to produce more layers for a fixed amount of money. Using low-diameter fibres increases the resolution, while decreasing the light yield per fibre and vice versa.

The active area of the detector consists of a total of four layers of Saint-Gobain BCF-12 1mm scintillating fibres. The fibres have an emission peak at 435nm, a decay time of 3.2ns and produce approximately 8000 photons per MeV. The core material of these fibres is PS (refractive index 1.60) while the cladding is made of PMMA (refractive index 1.49). The core includes a combination of fluorescent dopants responsible for the effect of scintillation, i.e. light production due to ionizing radiation.

A single layer consists of 64 fibres with a gap of 0.1mm between two neighbouring fibres. Fibres in the bottom two layers are parallel to each other, but shifted by a half period (0.55mm) with respect to each other as shown on figure 2.1. The fibres forming the top two layers are aligned in the same way as the fibres of the bottom layers. Top and bottom layer-pairs are then placed orthogonally to each other and fixed with the help of a two-part frame (141mm outer side length) as shown on figure 2.2. See drawings "Frame top" and "Frame bottom" in the appendix for complete dimensions.

2.2 SiPM arrays and housing

If a signal is produced inside a scintillating fibre, it has to be measured by a photodetector. The recent measurements done using a single SciFi plate and also the measurements of a future

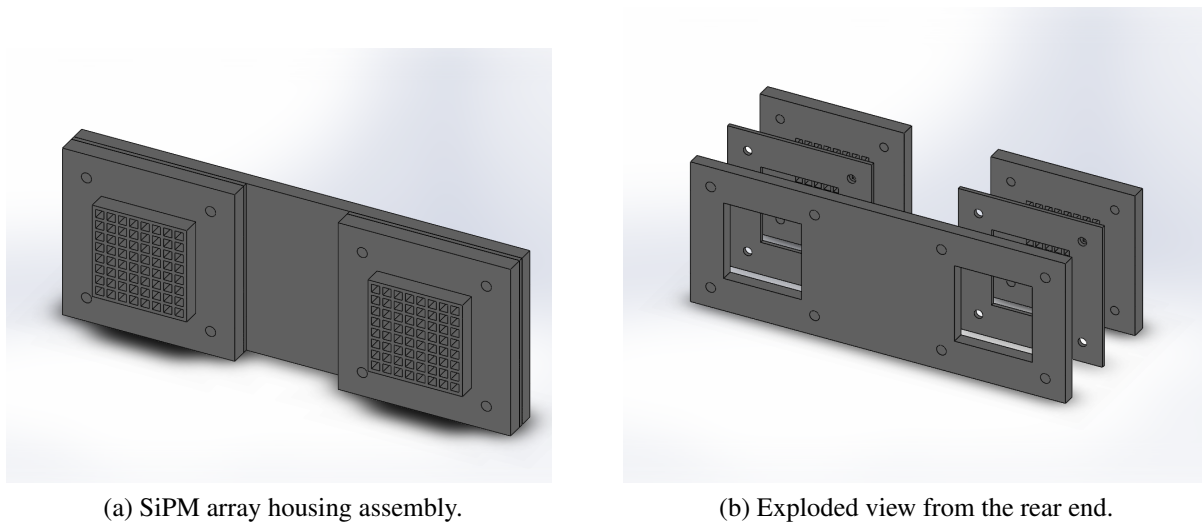


Figure 2.3: CAD model of Hamamatsu MPPC[®] array housing attached to a 130mm wide rear support.

muon telescope both operate using two Hamamatsu S13361-3050AE MPPC[®] modules. Each module consists of 8x8 SiPM arrays, each array being separated from its neighbouring array by a spacing of 0.2mm. A SiPM array itself is a collection of 3584 pixels, pixel pitch of 50 μ m with a total effective photosensitive area of 3x3mm. The spectral response ranges from 320nm to 900nm with a peak sensitivity wavelength of 450nm.

In order to create a fixed interface between the fibre ends and SiPM arrays, the fibres are grouped into bundles, each bundle containing four fibres, and drawn into a 3D printed socket described in figure 2.3. After the fibres have been fixed to the socket with epoxy and polished, the SiPM array modules are placed on top of the protruding fibres. The photodetectors are supported from the sides by another 3D printed frame and from the rear by a third 3D printed detail. Exact dimensions of the assembly can be found in drawings "Fibre socket", "SiPM array housing" and "SiPM rear support" from the appendix.

2.3 Rules of coincidence

In order to control our understanding of where a particle hits the detector, fibres are bundled into groups. One end is grouped together by bundling the fibres closest to each other, while the other end is grouped by bundling every fourth fibre (figure 2.4). The face of the first end of the bundle is placed on a single SiPM array with the help of the socket depicted in figure 2.3. The ends of each fibre of this four-bundle are then separated into four different windows on the other end. The process is repeated for every fibre.

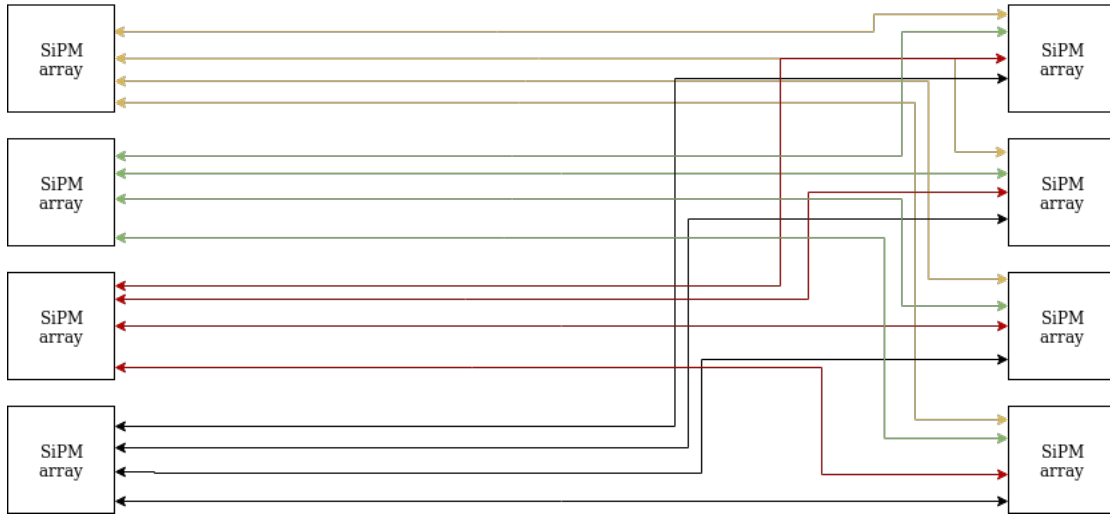


Figure 2.4: A schematic view of how fibres are bundled together. Each line represents a single fibre.

The result of this combination is described in tables 2.1 and 2.2 which document every single fibre that is drawn to its corresponding SiPM. The notation for each of the comma separated variables is <axis><layer><number of fibre>, e.g. xu20 refers to the 20th fibre of the upper ("u" stands for "up", "d" stands for "down") fibre layer of the x-axis. Shown in bold is an example of how a four-bundle connected to the left SiPM module is separated into four different arrays on the right module. The table illustrates that if two signals happen to be registered in both of the array modules in the arrays shown in yellow, the particle has hit the fibre yd1. This is due to the fact that fibre yd1 can only be measured by the SiPM arrays that in this illustration are shown in yellow.

Table 2.1: Individual fibre positions in the left interface.

xu20,xu24, xu28,xu32	xu19,xu23, xu27,xu31	xu18,xu22, xu26,xu30	xu17,xu21, xu25,xu29	xu4,xu8, xu12,xu16	xu3,xu7, xu11,xu15	xu2,xu6, xu10,xu14	xu1,xu5, xu9,xu13
xu52,xu56, xu60,xu64	xu51,xu55, xu59,xu63	xu50,xu54, xu58,xu62	xu49,xu53, xu57,xu61	xu36,xu40, xu44,xu48	xu35,xu39, xu43,xu47	xu34,xu38, xu42,xu46	xu33,xu37, xu41,xu45
xd20,xd24, xd28,xd32	xd19,xd23, xd27,xd31	xd18,xd22, xd26,xd30	xd17,xd21, xd25,xd29	xd4,xd8, xd12,xd16	xd3,xd7, xd11,xd15	xd2,xd6, xd10,xd14	xd1,xd5, xd9,xd13
xd52,xd56, xd60,xd64	xd51,xd55, xd59,xd63	xd50,xd54, xd58,xd62	xd49,xd53, xd57,xd61	xd36,xd40, xd44,xd48	xd35,xd39, xd43,xd47	xd34,xd38, xd42,xd46	xd33,xd37, xd41,xd45
yu33,yu34, yu35,yu36	yu37,yu38, yu39,yu40	yu41,yu42, yu43,yu44	yu45,yu46, yu47,yu48	yu49,yu50, yu51,yu52	yu53,yu54, yu55,yu56	yu57,yu58, yu59,yu60	yu61,yu62, yu63,yu64
yu1,yu2, yu3,yu4	yu5,yu6, yu7,yu8	yu9,yu10, yu11,yu12	yu13,yu14, yu15,yu16	yu17,yu18, yu19,yu20	yu21,yu22, yu23,yu24	yu25,yu26, yu27,yu28	yu29,yu30, yu31,yu32
yd33,yd34, yd35,yd36	yd37,yd38, yd39,yd40	yd41,yd42, yd43,yd44	yd45,yd46, yd47,yd48	yd49,yd50, yd51,yd52	yd53,yd54, yd55,yd56	yd57,yd58, yd59,yd60	yd61,yd62, yd63,yd64
yd1,yd2, yd3,yd4	yd5,yd6, yd7,yd8	yd9,yd10, yd11,yd12	yd13,yd14, yd15,yd16	yd17,yd18, yd19,yd20	yd21,yd22, yd23,yd24	yd25,yd26, yd27,yd28	yd29,yd30, yd31,yd32

Table 2.2: Individual fibre positions in the right interface.

yu20,yu24, yu28,yu32	yu19,yu23, yu27,yu31	yu18,yu22, yu26,yu30	yu17,yu21, yu25,yu29	yu4,yu8, yu12,yu16	yu3,yu7, yu11,yu15	yu2,yu6, yu10,yu14	yu1,yu5, yu9,yu13
yu52,yu56, yu60,yu64	yu51,yu55, yu59,yu63	yu50,yu54, yu58,yu62	yu49,yu53, yu57,yu61	yu36,yu40, yu44,yu48	yu35,yu39, yu43,yu47	yu34,yu38, yu42,yu46	yu33,yu37, yu41,yu45
yd20,yd24, yd28,yd32	yd19,yd23, yd27,yd31	yd18,yd22, yd26,yd30	yd17,yd21, yd25,yd29	yd4 ,yd8, yd12,yd16	yd3 ,yd7, yd11,yd15	yd2 ,yd6, yd10,yd14	yd1 ,yd5, yd9,yd13
yd52,yd56, yd60,yd64	yd51,yd55, yd59,yd63	yd50,yd54, yd58,yd62	yd49,yd53, yd57,yd61	yd36,yd40, yd44,yd48	yd35,yd39, yd43,yd47	yd34,yd38, yd42,yd46	yd33,yd37, yd41,yd45
xu33,xu34, xu35,xu36	xu37,xu38, xu39,xu40	xu41,xu42, xu43,xu44	xu45,xu46, xu47,xu48	xu49,xu50, xu51,xu52	xu53,xu54, xu55,xu56	xu57,xu58, xu59,xu60	xu61,xu62, xu63,xu64
xu1,xu2, xu3,xu4	xu5,xu6, xu7,xu8	xu9,xu10, xu11,xu12	xu13,xu14, xu15,xu16	xu17,xu18, xu19,xu20	xu21,xu22, xu23,xu24	xu25,xu26, xu27,xu28	xu29,xu30, xu31,xu32
xd33,xd34, xd35,xd36	xd37,xd38, xd39,xd40	xd41,xd42, xd43,xd44	xd45,xd46, xd47,xd48	xd49,xd50, xd51,xd52	xd53,xd54, xd55,xd56	xd57,xd58, xd59,xd60	xd61,xd62, xd63,xd64
xd1,xd2, xd3,xd4	xd5,xd6, xd7,xd8	xd9,xd10, xd11,xd12	xd13,xd14, xd15,xd16	xd17,xd18, xd19,xd20	xd21,xd22, xd23,xd24	xd25,xd26, xd27,xd28	xd29,xd30, xd31,xd32

2.4 DAQ

Our readout system is provided by CAEN S.p.A. The hardware is physically separated into two: a motherboard (DT5550W) and a piggyback (A55PET4). The evaluation board is based on Weeroc's Petiroc 2A model of application-specific integrated circuits (ASIC), dedicated for SiPM readout and processing the analog signal. The board comes with user friendly readout software, but also includes a software package – SCI-Compiler – for custom firmware development.

The motherboard contains a Xilinx model XC7K160T field-programmable gate array (FPGA), an ADC and external connectors. It is responsible for processing the digitized signals coming from ASICs and the interface with the host PC.

The piggyback board hosts four ASICs responsible for SiPM readout, each ASIC integrating 32 readout channels. It also hosts a SiPM power supply (CAEN A7585D), MPPC connectors (Samtec SS4-40-3.00-L-D-K-TR), a temperature sensor and a mezzanine connector to plug the piggyback board onto the motherboard.

The SiPM array modules are attached directly to the piggyback board and the fibres are firmly connected with the help of a 3D printed detail shown in figure 2.3. The board is placed vertically in order to keep the SciFi plate horizontal. The board has a maximum recommended operating temperature of 50°C, but has to be placed into a sealed box since the SciFi plate has to remain protected from external light sources. This issue is solved by placing the system into a spacious (in our case 90 litre) box with a Peltier element attached to the upper side of the box. This system kept the temperature below 40°C at all times.

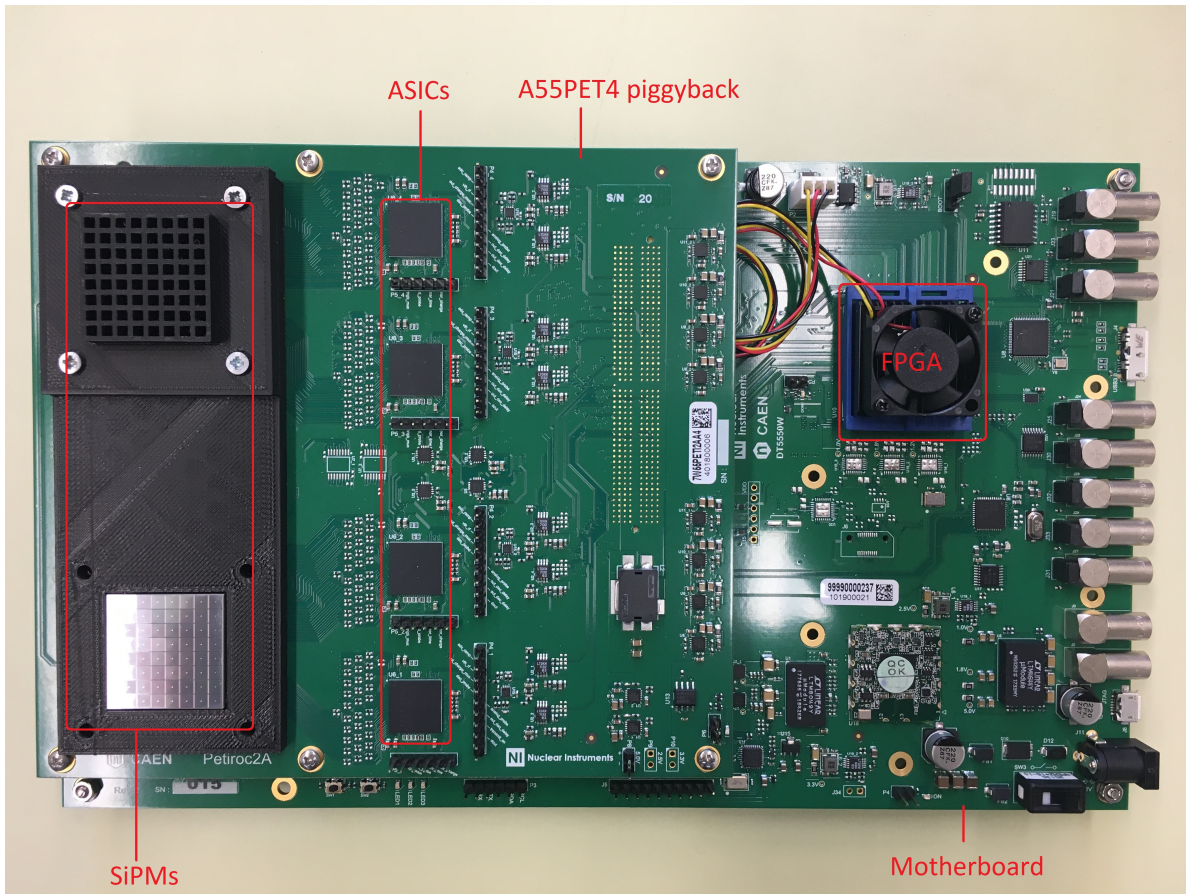


Figure 2.5: DAQ board shown with one MPPC exposed and the other covered with a socket that will house the fibre bundles.

2.5 Muon telescope

As a bonus, the existing detector design can be expanded into a cosmic ray muon telescope in the near future. The main difference between the existing detection device and a telescope is the fact that instead of having only a single detection plate, a telescope has two identical plates stacked on top of each other. This means that a telescope can better recognize cosmic ray muons from other ionizing radiation. Without two detection plates, it is difficult to differentiate between muons and secondary electrons that are continuously created.

The number of fibres and frames have to be doubled, yet the number of SiPM arrays and readout boards can remain the same. The current SiPM arrays have enough area to fit up to nine fibres on them. A cosmic ray telescope would therefore need new fibre sockets that can house eight fibres in a single window. SiPM interfaces have to be placed symmetrically as depicted in figure 2.6. Additionally the rules of coincidence have to be modified to take into account the coincidences that occur in different plates.

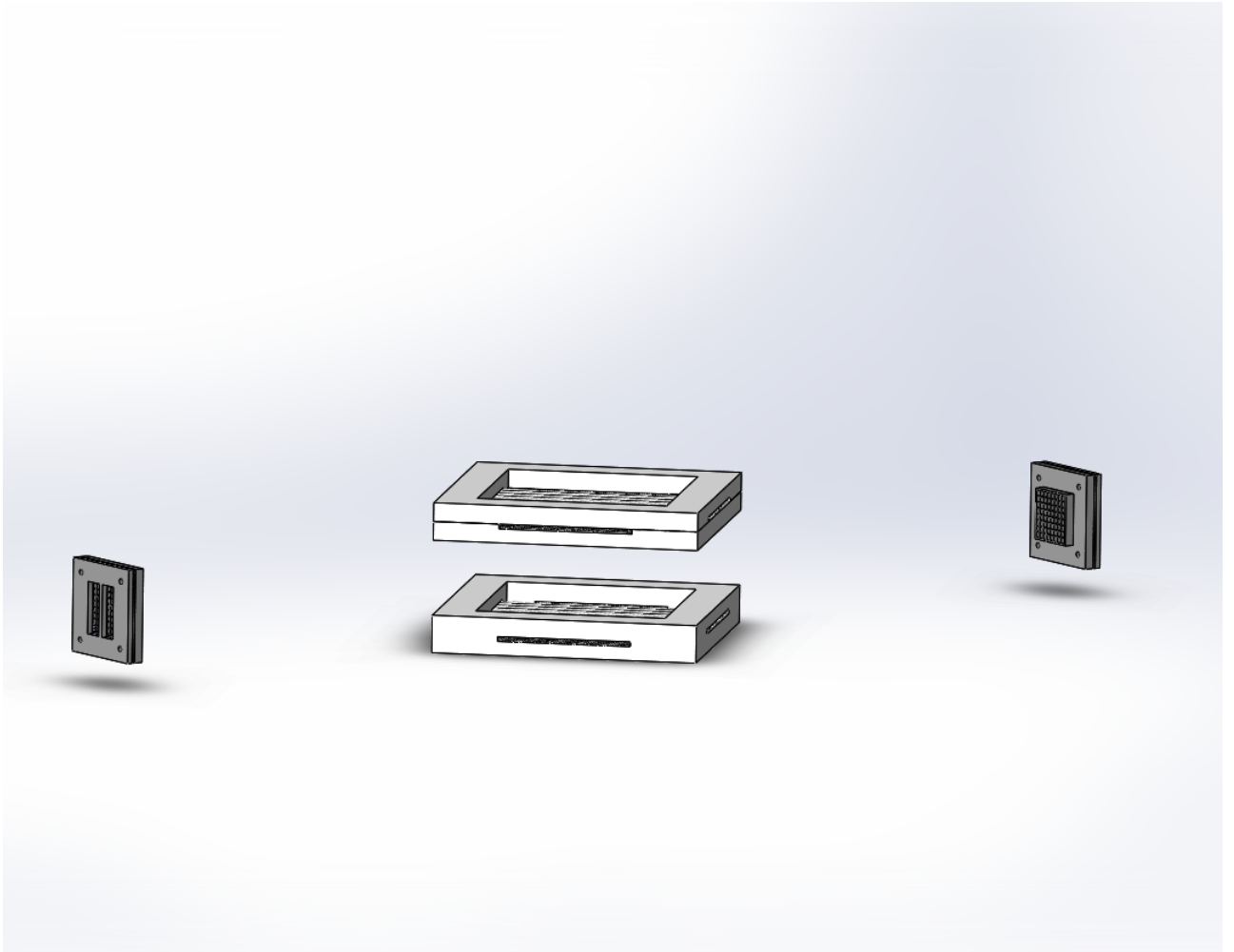


Figure 2.6: The concept of a muon telescope. Fibres outside the active area are not depicted.

Chapter 3

Experimental progress

The amount of time it takes to prepare a physical prototype of a muon detector is inflated by a number of factors: the waiting times are long for ordering DAQ devices, photodetectors and scintillating fibres; drying and curing times of the various chemicals used in the experiments are long; most of the mechanical details have to be custom made. Furthermore, developing the physical device was preceded by a long period of computer simulations that shaped our design decisions. Finally, before anything else could be assembled, epoxy moulding and removal techniques had to be developed. Due to these factors the development of a physical system has only recently started to gain momentum. Below is an overview of the experimental improvements that have taken place in the last four months.

3.1 Fibres

The fibres used in this project are all plastic fibres with a circular cross-section and a diameter of 1mm. Various types of fibres were used in creating dummy (non-scintillating, experimentally unusable) fibre plates, including both PMMA and PS optical fibres. It was determined that PMMA is not a good option in our current experimental setup due to the fact that its mechanical properties do not enable the manipulation of the fibres into a proper plate *without* straightening the fibres beforehand by using special machinery.

The final detection plate described in this chapter was made using scintillating wavelength-shifting PS fibres produced by Saint-Gobain; the full telescope itself however will likely be created from similar fibres produced by Kuraray. The fibres are surrounded by cladding that has a lower refractive index compared to the core of the fibres. The cladding therefore promotes total internal reflection and is responsible for reducing the light that escapes the fibres.

Each fibre is initially cut to a length of 1m. The size of the fibres is eventually slightly reduced due to further cutting and polishing. Cut fibres are then aligned from one end and grouped to bundles of 10 and 7 with a piece of tape. A single layer of fibres on a detection plate contains 64 fibres which is achieved by placing five bundles of 10 and two bundles of 7 fibres on the aligning table.

3.2 Assembling the fibre mats

Many different attempts were made to assemble mats of scintillating fibres. The process of determining an optimal way of preparing a small (10 cm²) fibre mat happened in four stages: experimenting with different epoxies and how they perform with aluminium, preparing a single-layer dummy, preparing a multilayer dummy and finally assembling a fibre mat with real scintillating fibres.

3.2.1 Preparing the aligning table

Before any significant number of fibres were assembled, moulding and removal techniques of the fibre mat had to be developed. The aluminium plate (fig. 3.1) for moulding was prepared by Protolab and includes V-shaped grooves with a step size of 1.1 ± 0.2 mm and a depth of 0.4 ± 0.1 mm. Epoxy can easily be removed from the plate only if the aluminium is treated correctly beforehand. Treatment starts by removing any resin that is left from previous mouldings by cleaning it with a solvent. In this work a mixture of toluene and methyl ethyl ketone was used for the initial cleaning. After the cleaning procedure the plate has to be treated with a sealer, e.g. Mikon® 699 by Münch Chemie or Loctite Frekote® B-15 by Henkel. The sealing compound is needed to seal any microscopic pores or imperfections on the aluminium aligning plate.

Finally, few (4-6) layers of release agent have to be applied. Each layer should dry for at least half an hour while the final layer should have time to cure for a few hours. The release agents are needed to prevent the epoxy from adhering to the moulding plate. Applying too few layers of release agent or forgetting to apply it after cleaning the surface with a solvent can result in breaking the fibre mat during the removal from the aligning plate. Two different release agents were used in the work described in this thesis: Mikon® 705 from Münch Chemie and Loctite® Frekote 700-NC from Henkel. Both work equally well.

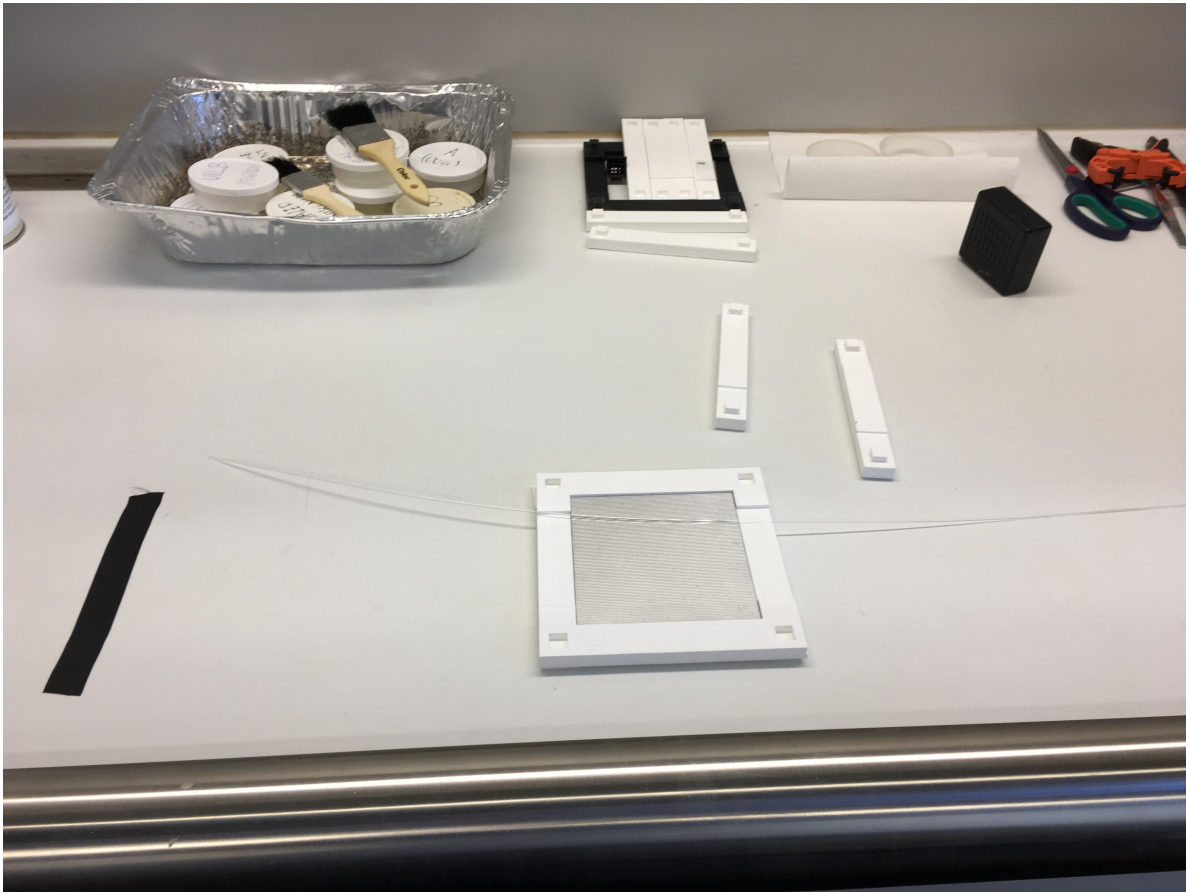


Figure 3.1: A single fibre next to the prepared Al aligning table before any epoxy has been applied.

3.2.2 Preparing the epoxy

The epoxy that is used to hold the fibres together was chosen due to its relatively low viscosity. A high viscosity resin would potentially not fill the gaps between the individual fibres and fibre layers.

During the process of mixing resin with hardener, a small amount of TiO_2 was also added to the epoxy mixture as suggested by the papers describing the SciFi upgrade in the LHCb detector [15, 16]. TiO_2 absorbs UV light, thereby reducing any potential crosstalk between neighbouring fibres in the active area of the scintillation plate. MgCO_3 was tried as well, however it did not mix uniformly enough to continue working with it. Solvents were also used to help the mixing procedure, but this will ruin the quality of the epoxy.

3.2.3 Aligning the fibres

Through trial and error we found that it is best to cover the aluminium base plate with an initial layer of epoxy before any fibres are put in their place. The fibres are grouped into bundles of ten or less, making sure that the ends of fibres remain aligned. Each bundle is then attached to the aluminium plate with the help of the very first layer of epoxy. If the number of fibres reaches 64, a small amount of epoxy is again brushed on the active area of fibres to make sure that the 0.1mm gaps between the fibres are filled.

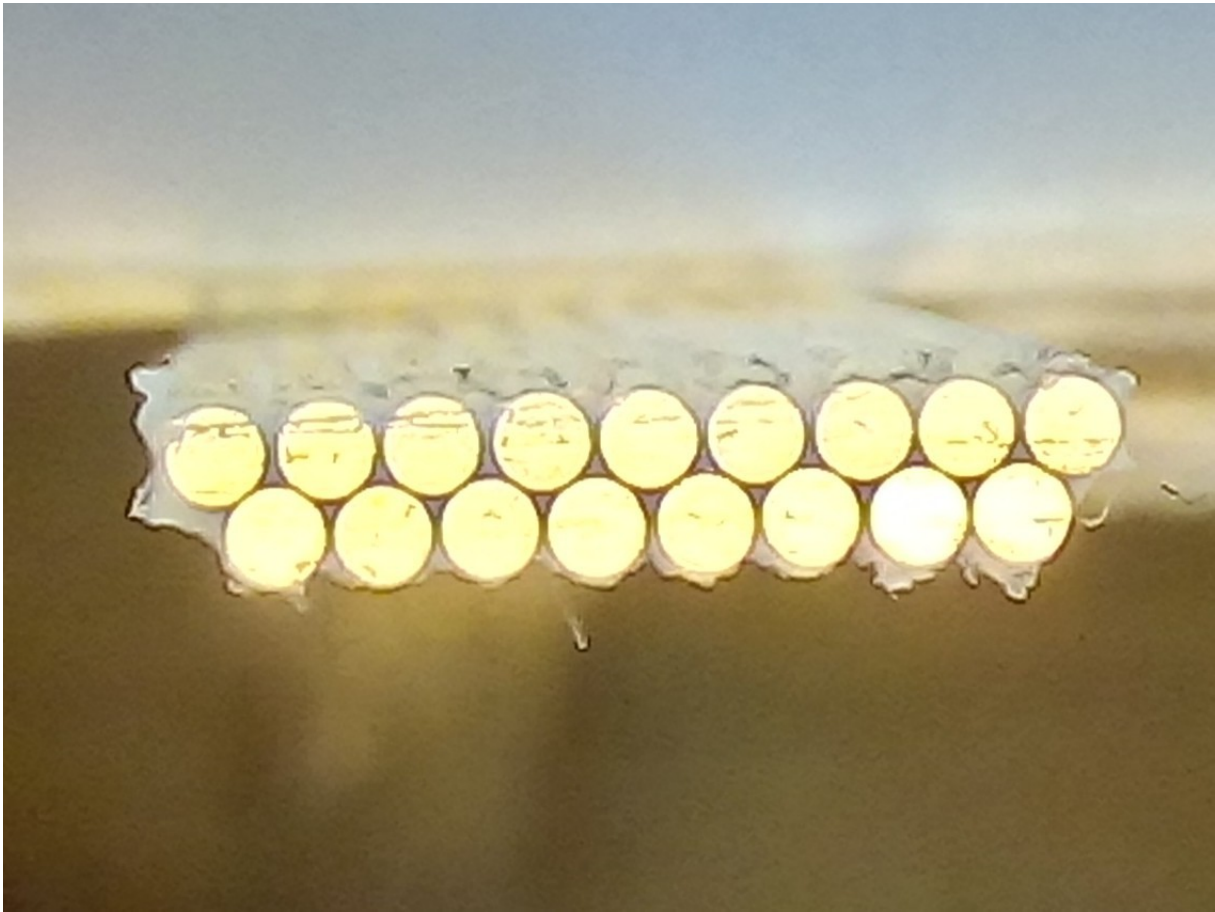
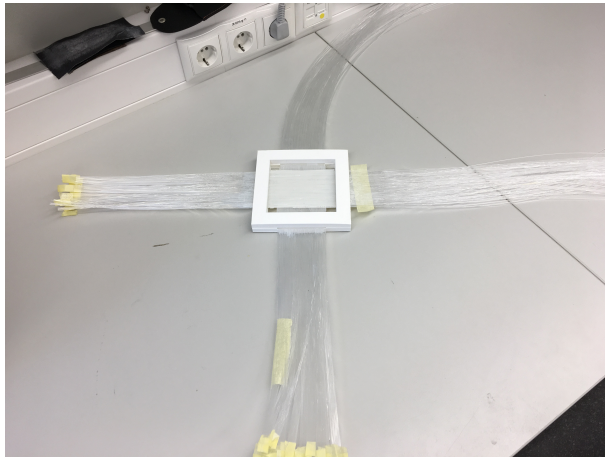
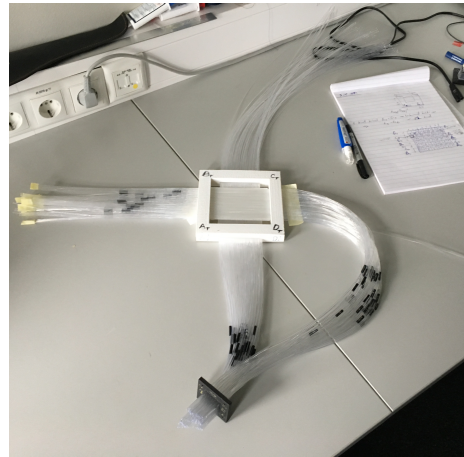


Figure 3.2: Cross-sectional view of a dummy fibre mat consisting of 17 PS fibres.

After the first layer has cured for a few hours, a second layer is put on the first layer in a similar fashion. The only difference is that the first layer is aligned using the aluminium alignment table, whereas the second layer is aligned with the help of the first layer itself. The resulting structure can be seen in figure 3.2. After the two pairs of double layer fibres are cured and removed, they are placed orthogonally with respect to each other as depicted in figure 3.3.



(a) A scintillating fibre plate after the epoxy has cured.



(b) A detector plate with the first fibre bundles collared, labelled and connected to the SiPM interface.

Figure 3.3: Post-curing procedures.

3.3 Connecting fibres to SiPM arrays

Every fibre-end is grouped into a bundle of four fibres. Fibres of the shorter end are grouped with their closest neighbours. Fibres of the longer end are grouped together with the fourth fiber next to it, e.g. fibres 1, 5, 9 and 13 are grouped together. Every bundle is collared and labelled using a 3D printed detail that fits no more than four fibres.

The small windows inside the sockets have to be sanded and checked with a dummy fibre bundle. Pressing the fibres into an ill-fitting socket can cause the fibres to strain. Finally, bundles of four are pushed into the socket.

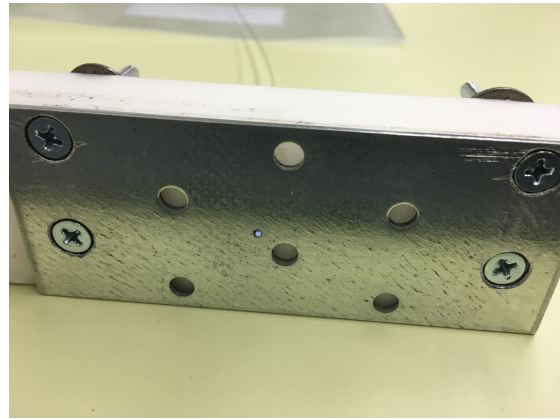
3.4 Polishing

The way our fibres are polished is inspired by already existing methods. Still, the tools of polishing had to be developed by ourselves due the fact that we did not find any existing tools from anywhere in Estonia. Laboratories and companies in Estonia concerned with fibre optics tend to work with glass fibres and the tools used in manipulating glass fibres do not fit together with the tools used to manipulate plastic fibres. Multiple variations of the final technique were studied, until through trial and error the best way was found.

The initial technique of polishing PS fibres was implemented for polishing individual fibres only. Polishing fibres individually meant that we could quickly study the effects of polishing on



(a) A lapping film next to the polishing tool.



(b) The underside of the polishing tool.

Figure 3.4: Polishing the fibres individually.

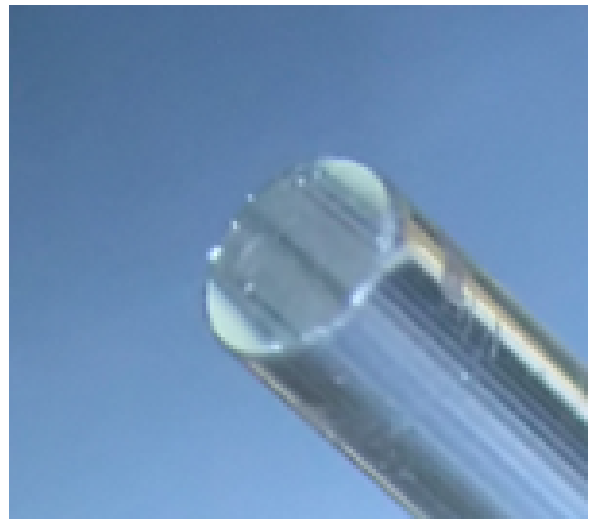
a single fibre under an optical microscope. As seen in figure 3.4, the custom polishing tool is a simple block of Teflon with an aluminium plate attached to it. Teflon is chosen in order to not damage the fibre cladding and the aluminium plate is needed to keep the Teflon from wearing down during the sanding process. A 1mm-diameter PS fibre is pulled through the 1.5mm hole in the center of the tool which helps to keep the fibre in place and also aligns the end of the fibre correctly. The fibre is fixed with the help of a silicone sealant.

Although polishing individual fibres proved that using a manual method consisting of gradually changing lapping films is good for improving the ends of scintillating fibres, polishing hundreds of fibres individually would take an unreasonable amount of time. Additionally, the fibres have to be cut and polished again after they have been glued to the 3D-printed interface. Therefore, a way of polishing the fibres in bulk had to be developed.

The final method of polishing used in preparing the first working scintillating fibre plate involves using the 3D-printed SiPM array interface itself. After the fibres have been correctly inserted and glued into the SiPM interface, a small part (a few millimeters) of the fibre end will protrude from the other side of the interface. The interface is placed into a polishing rack with the help of a 3D-printed tool (drawing "Polishing support" in the appendix) that exposes the back-side of the interface, leaving the rear end of the 3D-printed interface parallel to horizontal Teflon plate. The interface is then treated with different grade sandpapers (P800, P1000, P1200, P1500, P2000, P2500) and lapping films ($5\mu\text{m}$, $2\mu\text{m}$, $1\mu\text{m}$).

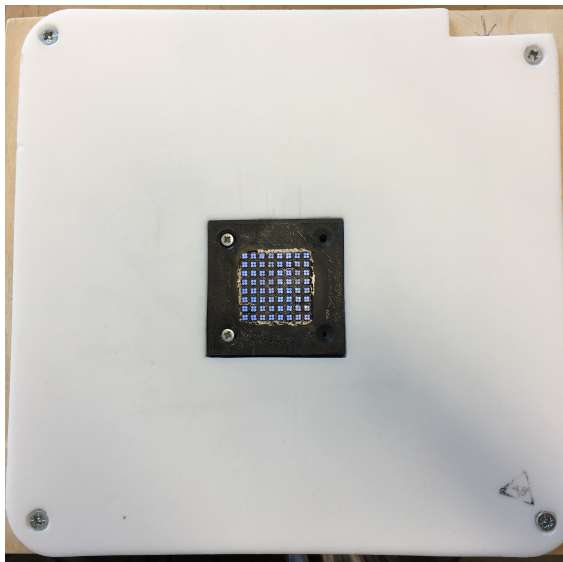


(a) Unpolished scintillating fibre.

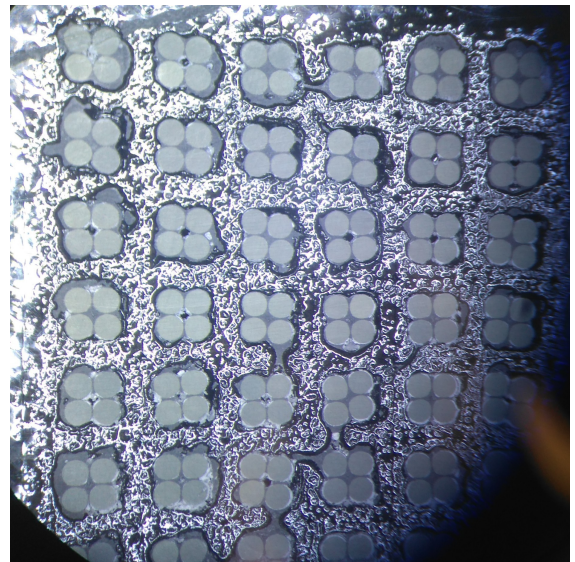


(b) Polished fibre.

Figure 3.5: Result of the polishing procedure as seen under an optical microscope.



(a) A SiPM interface pressed into the polishing table.

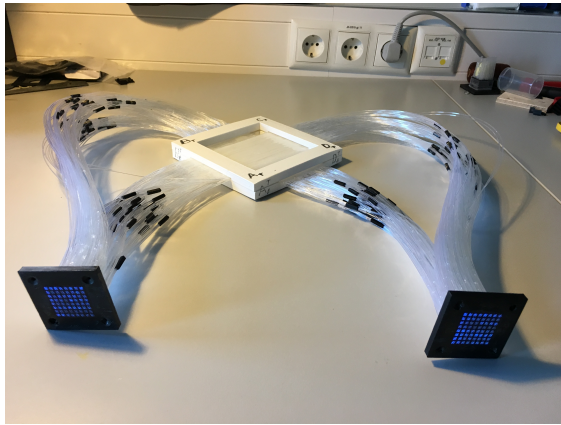


(b) Fixed and polished fibres under an optical microscope.

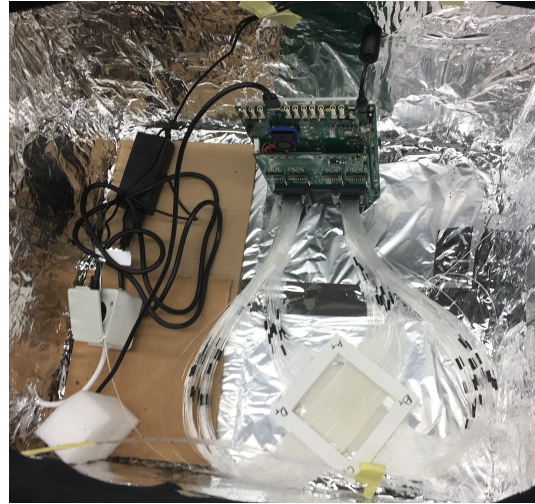
Figure 3.6: The final polishing method.

3.5 The working system

After both of the interfaces have been epoxied and polished, they are bolted to the DAQ board together with the photodetectors. The system is placed into a light tight box and data acquisition can start. The final experimental setup can be seen in figure 3.7b.

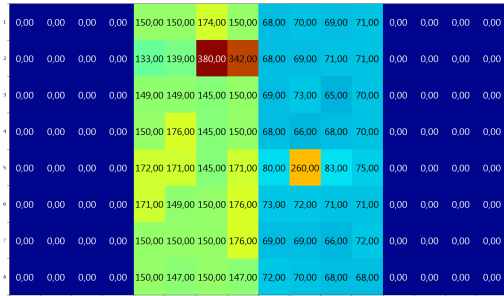


(a) A SciFi plate removed from the polishing rack and ready for measurements.

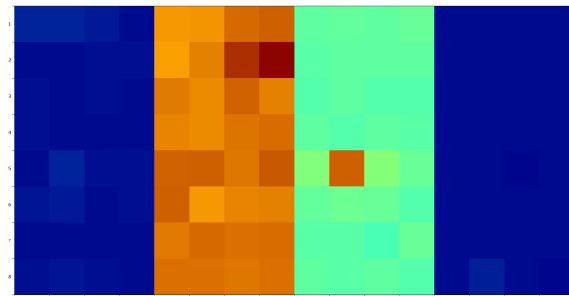


(b) Fully assembled detector.

Figure 3.7: Final steps before data acquisition.



(a) Real time view.



(b) Accumulated signals.

Figure 3.8: Measurements using an UV source attached to a single fibre.

Initial measurements without any fibres attached to the photodetectors and the succeeding measurements with our detection plate attached showed that the surrounding box eliminated any light and that the fibres are indeed producing signals due to surrounding ionizing particles.

Figure 3.8 demonstrates the position sensitivity of the device. Shown are the real time view as well as the cumulative view of the signals that are produced if an UV LED is attached to a single fibre. The left half of both figures 3.8a and 3.8b represents the channels of the two ASICs

connected to one of the SiPM array modules and the right half corresponds to the other two ASICs. On figure 3.8b, comparing both the strongest signal of the left SiPM and the strongest signal of the right SiPM, one can conclude which fibre produced this signal with the help of the map described in tables 2.1 and 2.2. In this specific case the fibre was xu37, i.e. the 37th fibre of the upper layer of the x-axis.

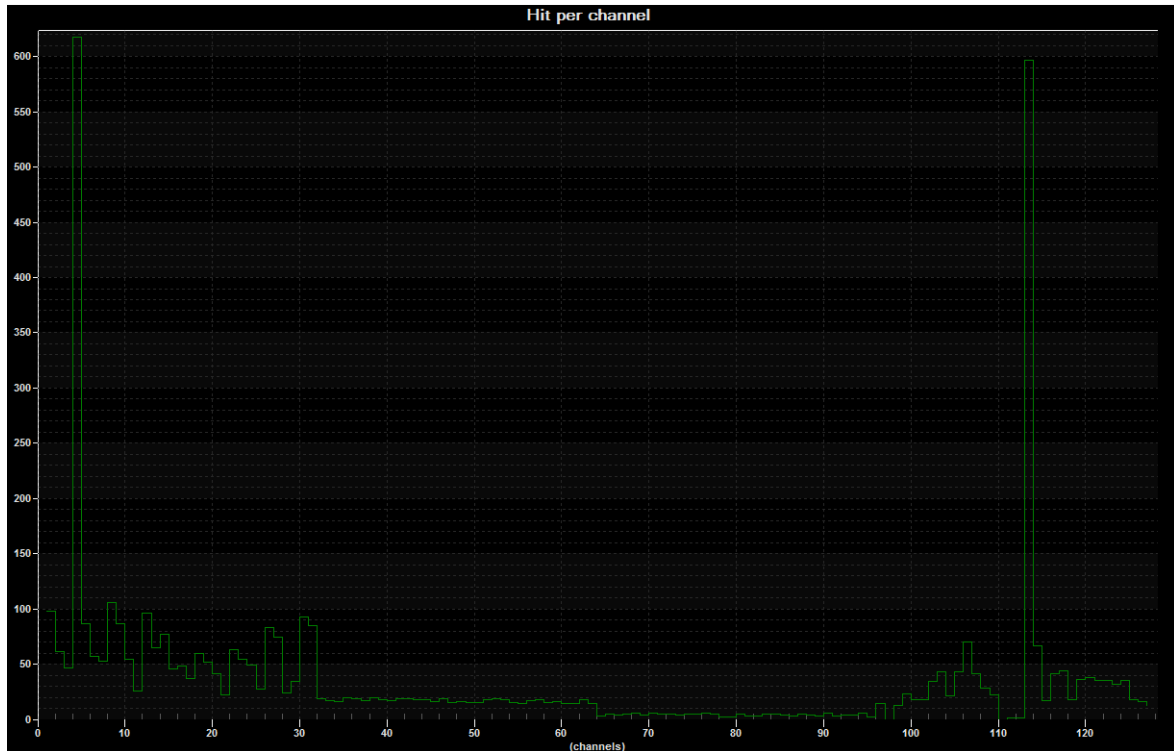


Figure 3.9: Hits per channel; UV source attached to a single fibre.

Figure 3.9 further demonstrates the position sensitivity. Another single fibre is attached to the same UV source and one can clearly see two peaks corresponding to two SiPM arrays, originating from the same fibre. The signals are time stamped and can be accumulated either visually and/or saved into a text format for further processing.

3.6 Open issues

Problems to be solved in the near future include, but are not limited to, reducing the air bubbles that creep in during the epoxy mixing process, finding a way to mix TiO_2 more uniformly, increasing the speed and quality of applying scintillating fibres. The current fibre-SiPM interface is made of PLA and contains 0.4mm thick walls that separate fibre bundles; a SiPM housing that does not break if only a 200 μm separating wall is used would be necessary if 8-fibre bundles were to be implemented. A large number of issues are also related to the fact

that the current detection plate build process was in large part manual work. The human factor not only makes the work very slow but also increases various errors, such as aligning the fibres incorrectly, using a wrong number of fibres, straining the fibres and damaging the cladding.

In order to make the system more mobile, optical sealing techniques should be developed. The current solution is to put the whole system inside a box, but a more practical solution would be to shield the active area and the fibre bundles separately. A more robust system would also need a dedicated chassis and cooling system to operate outside a well ventilated and air-conditioned room.

The current interface between fibres and photodetectors has very clear drawbacks: drawing the fibres from the active area to the SiPM arrays results in a lot of wasted scintillating fibre, i.e. expensive fibre that only acts as a light guide and is not actually used in the active region. A potential solution for this problem would be to place SiPM array rows right next to the active region and therefore surround detection plates with SiPM modules.

Further problems need to be solved if the project reaches a point where a full size tomograph will be developed. More ambitious detection devices need an automated method of assembling the fibre mats; alternatively, fibre mats could be replaced by solid scintillating plates to avoid the problems that come with using individual fibres. Concerns also stem from the fact that expanding the active area of the detector increases the weight of active area. This could make the active area lose its current shape and deform the detection plane into a Gaussian shape. If any support structures are added, uniformity of detection plane's composition will be lost.

Conclusion

Inspired by modern muon tomographic devices as well as other scintillating fibre detectors, a miniature cosmic ray detector has been designed and implemented. The work demonstrates a method of how a scintillating fibre cosmic ray detection plate can be designed along with the photodetectors and readout electronics needed for it operate. Furthermore, the design allows for the existing system to be relatively easily extended into a cosmic ray telescope in the future.

The experimental work consisted of building a functioning particle detector and developing the assembly techniques needed. As a result, we have gained a better understanding of what would reasonable photodetector configurations be and how to construct the active scintillating regions of any future detectors. The work also answered multiple previously open practical questions, such as how to create an epoxy mould, how to align the fibres and how to connect them to a photodetector. Besides gaining useful know-how, the work also raised many questions that are yet to be solved if more ambitious detectors were to be built.

Acknowledgements

I would like to thank my supervisors Madis Kiisk and Anzori Georgadze for their support throughout the work done for this thesis. Without the materials, tools, guidance and help provided by them, building such a device would not have been possible. The work was made financially possible by GoSwift OÜ. The 3D prints used in the thesis were made possible thanks to Ivo Romet and Teet Tilk. Finally, I am grateful for the discussions and suggestions given by the people who have been working on other aspects of this project: Märt Mägi, Egils Avots, Gholamreza Anbarjafari and Aivo Anier.

Bibliography

- [1] K. N. Borozdin, G. E. Hogan, C. Morris, W. C. Priedhorsky, A. Saunders, L. J. Schultz, and M. E. Teasdale. Surveillance: Radiographic imaging with cosmic-ray muons. *Nature*, 422(6929):277–277, 2003.
- [2] S. Pesente, S. Vanini, M. Benettoni, G. Bonomi, P. Calvini, P. Checchia, E. Conti, F. Gonella, G. Nebbia, S. Squarcia, G. Viesti, A. Zenoni, and G. Zumerle. First results on material identification and imaging with a large-volume muon tomography prototype. *Nuclear Instruments and Methods in Physics Research Section A: Accelerators, Spectrometers, Detectors and Associated Equipment*, 604(3):738 – 746, 2009.
- [3] K. Gnanvo, L. V. Grasso, M. Hohlmann, J. B. Locke, A. Quintero, and D. Mitra. Imaging of high-Z material for nuclear contraband detection with a minimal prototype of a muon tomography station based on gem detectors. *Nuclear Instruments and Methods in Physics Research Section A: Accelerators, Spectrometers, Detectors and Associated Equipment*, 652(1):16 – 20, 2011. Symposium on Radiation Measurements and Applications (SORMA) XII 2010.
- [4] J. Marteau, D. Gibert, N. Lesparre, F. Nicollin, P. Noli, and F. Giacoppo. Muons tomography applied to geosciences and volcanology. *Nuclear Instruments and Methods in Physics Research Section A: Accelerators, Spectrometers, Detectors and Associated Equipment*, 695:23 – 28, 2012. New Developments in Photodetection NDIP11.
- [5] G. Jonkmans, V. N. P. Anghel, C. Jewett, and M. Thompson. Nuclear waste imaging and spent fuel verification by muon tomography. *Annals of Nuclear Energy*, 53:267 – 273, 2013.
- [6] M. Bandieramonte, F. Vitello, V. A. De Logu, U. Becciani, A. Costa, S. Riggi, C. Pistagna, C. Pugliatti, D. L. Presti, F. Riggi, P. Rocca, F. Longhitano, P. Massimino, C. Petta, G. Santagati, G. Fallica, M. Belluso, and G. Bonanno. The Muon Portal Project: Development of an innovative scanning portal based on muon tomography. 06 2013.
- [7] D. F. Mahon, A. Clarkson, D. J. Hamilton, M. Hoek, D. G. Ireland, J. R. Johnstone,

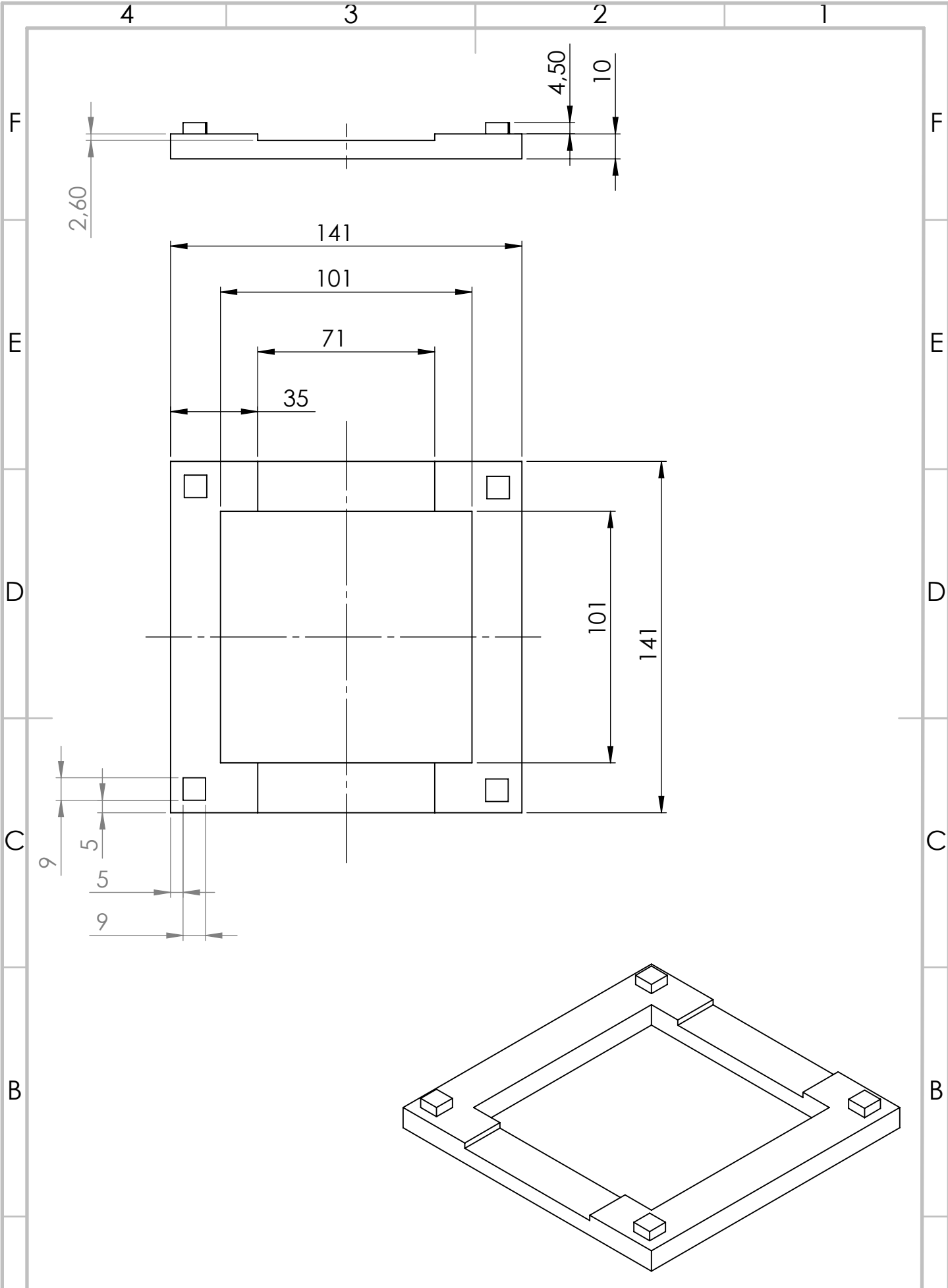
- R. Kaiser, T. Keri, S. Lumsden, B. McKinnon, M. Murray, S. Nutbeam-Tuffs, C. Shearer, C. Staines, G. Yang, and C. Zimmerman. A prototype scintillating-fibre tracker for the cosmic-ray muon tomography of legacy nuclear waste containers. *Nuclear Instruments and Methods in Physics Research Section A: Accelerators, Spectrometers, Detectors and Associated Equipment*, 732:408 – 411, 2013. Vienna Conference on Instrumentation 2013.
- [8] C. L. Morris, A. Saunders, M. J. Sossong, L. J. Schultz, J. A. Green, K. N. Borozdin, N. W. Hengartner, R. A. Smith, J. M. Colthart, D. C. Klugh, et al. Imaging and sensing based on muon tomography, October 16 2012. US Patent 8,288,721.
- [9] M. Mägi, G. Anbarjafari, A. S. Georgadze, M. Kiisk, E. Avots, and S. Suurpere. Prototype development of cosmic-ray tomography for hazardous materials detection. <https://www.etis.ee/Portal/Projects/Display/4a650e1e-1b91-4c53-b4b3-01f022326df0?lang=ENG>, 2017-2018.
- [10] M. Kiisk, G. Anbarjafari, Aivo Anier, A. S. Georgadze, M. Mägi, E. Avots, and S. Suurpere. Development of a polystyrene-based scintillation fiber-mat telescope for cosmic ray detection. <https://www.etis.ee/Portal/Projects/Display/794afb35-253b-4c6c-a39f-179ae9829041?lang=ENG>, 2019.
- [11] M. Tanabashi et al. Review of particle physics. *Physical Review D*, 98(3), 8 2018.
- [12] L. J. Schultz, K. N. Borozdin, J. J. Gomez, G. E. Hogan, J. A. McGill, C. L. Morris, W. C. Priedhorsky, A. Saunders., and M. E. Teasdale. Image reconstruction and material Z discrimination via cosmic ray muon radiography. *Nuclear Instruments and Methods in Physics Research Section A: Accelerators, Spectrometers, Detectors and Associated Equipment*, 519(3):687–694, 2004.
- [13] G. Blanpied, S. Kumar, D. Dorroh, C. Morgan, I. Blanpied, M. Sossong, S. McKenney, and B. Nelson. Material discrimination using scattering and stopping of cosmic ray muons and electrons: Differentiating heavier from lighter metals as well as low-atomic weight materials. *Nuclear Instruments and Methods in Physics Research Section A: Accelerators, Spectrometers, Detectors and Associated Equipment*, 784:352 – 358, 2015. Symposium on Radiation Measurements and Applications 2014 (SORMA XV).
- [14] A. Clarkson, D. J. Hamilton, M. Hoek, D. G. Ireland, J. R. Johnstone, R. Kaiser, T. Keri, S. Lumsden, D. F. Mahon, B. McKinnon, M. Murray, S. Nutbeam-Tuffs, C. Shearer, C. Staines, G. Yang, and C. Zimmerman. The design and performance of a scintillating-fibre tracker for the cosmic-ray muon tomography of legacy nuclear waste containers. *Nuclear Instruments and Methods in Physics Research Section A: Accelerators, Spectrometers, Detectors and Associated Equipment*, 745:138 – 149, 2014.

- [15] C. Joram, U. Uwer, T. Kirn, B. D. Leverington, S. Bachmann, R. J. Ekelhof, and J. Müller. LHCb scintillating fibre tracker engineering design review report: Fibres, mats and modules. Technical report, 2015.
- [16] P. Hopchev. Scifi: A large scintillating fibre tracker for LHCb. *arXiv preprint arXiv:1710.08325*, 2017.

Appendix A

Drawings

Multiple mechanical details used in either the already built detection plate or in the future telescope are created using a 3D printer. Below are drawings of all the details that had to be designed and printed for this project.



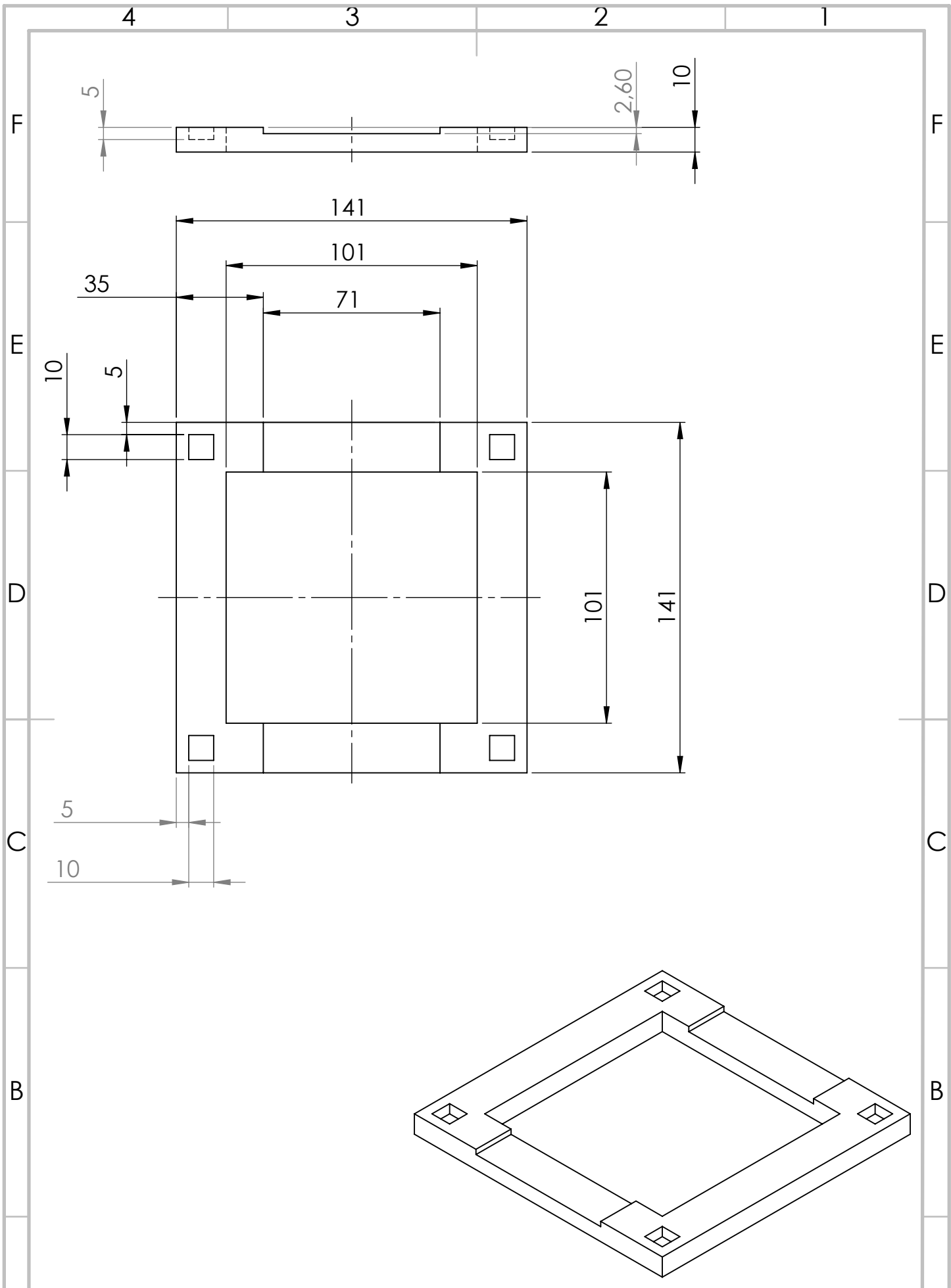
UNLESS OTHERWISE SPECIFIED: DIMENSIONS ARE IN MILLIMETERS

NAME		MATERIAL:	PLA
DRAWN	Sander Suurpere		
CHK'D	Madis Kiisk		

TITLE: **Frame bottom**

SCALE: 1:2

SHEET 1 OF 1



A

UNLESS OTHERWISE SPECIFIED: DIMENSIONS ARE IN MILLIMETERS

NAME		TITLE:	<h1>Frame top</h1>	
DRAWN	Sander Suurpere	MATERIAL:		PLA
CHK'D	Madis Kiisk	SCALE:1:2		SHEET 1 OF 1

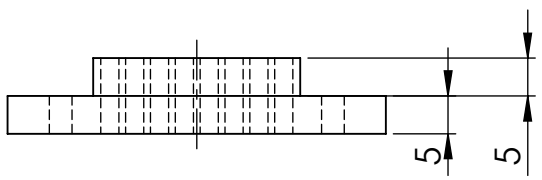
A



4 3 2 1

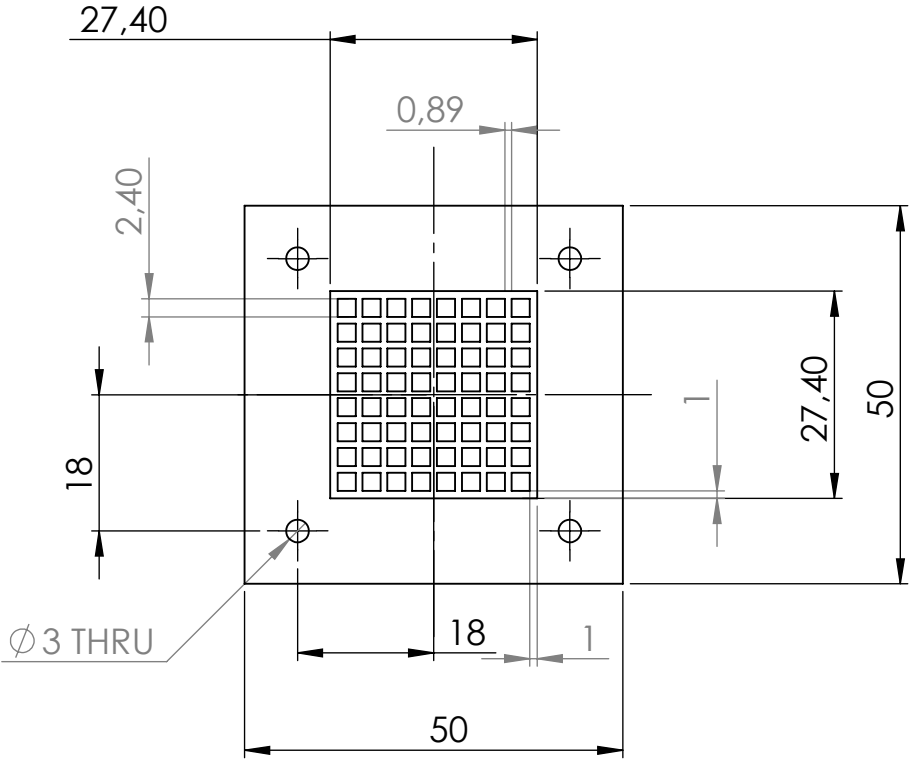
F

F



E

E

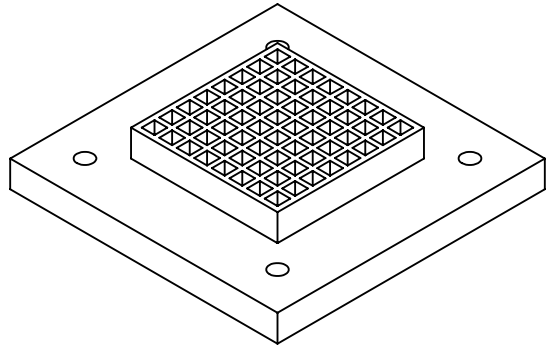


D

D

C

C



B

B

A

A

UNLESS OTHERWISE SPECIFIED: DIMENSIONS ARE IN MILLIMETERS

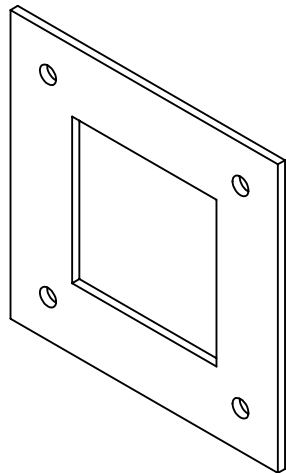
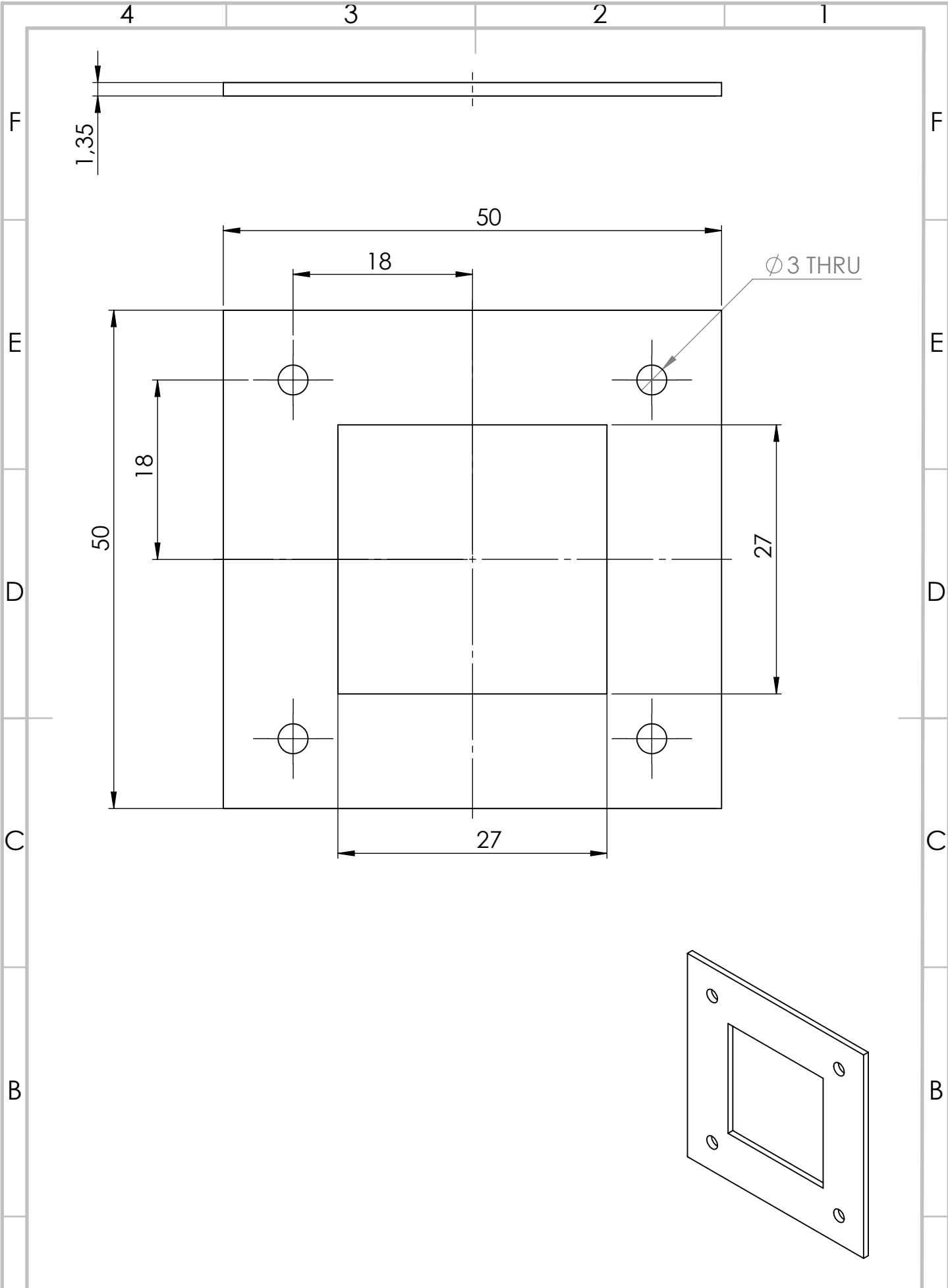
NAME		MATERIAL:	PLA
DRAWN	Sander Suurpere		
CHK'D	Madis Kiisk		

TITLE: **Fibre socket**

SCALE: 1:1

SHEET 1 OF 1

4 3 2 1



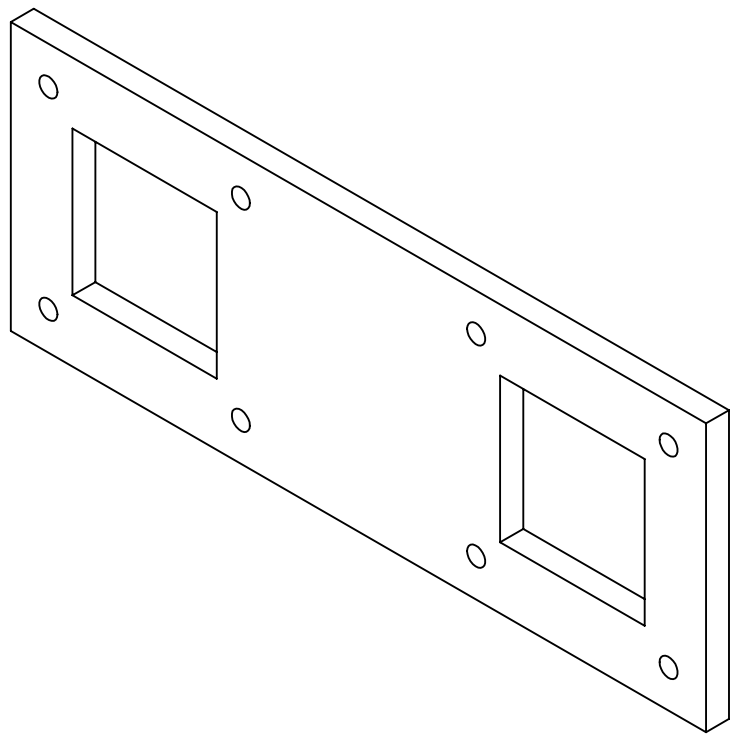
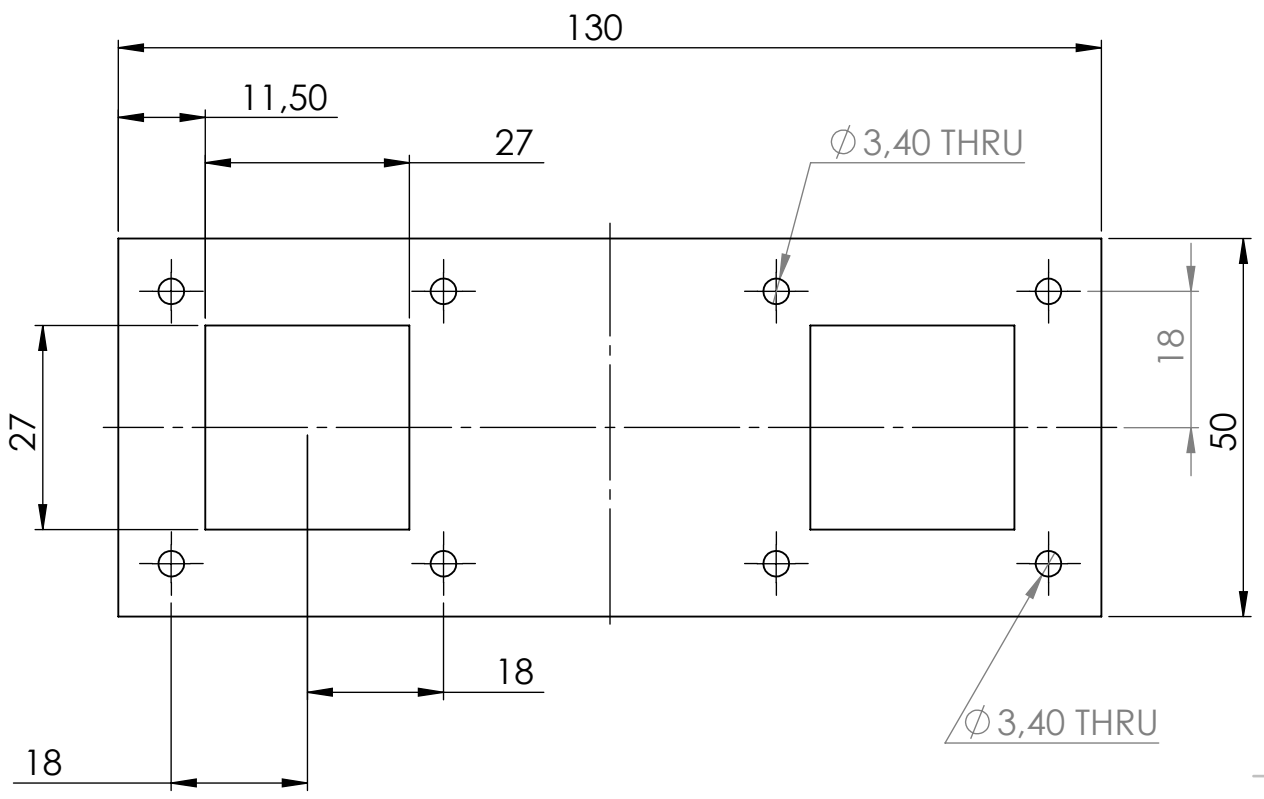
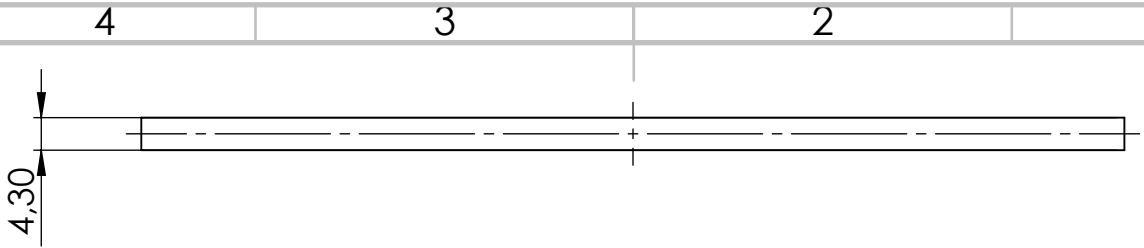
UNLESS OTHERWISE SPECIFIED: DIMENSIONS ARE IN MILLIMETERS

NAME		MATERIAL:	PLA
DRAWN	Sander Suurpere		
CHK'D	Madis Kiisk		

TITLE:
SiPM array housing

SCALE:2:1

SHEET 1 OF 1



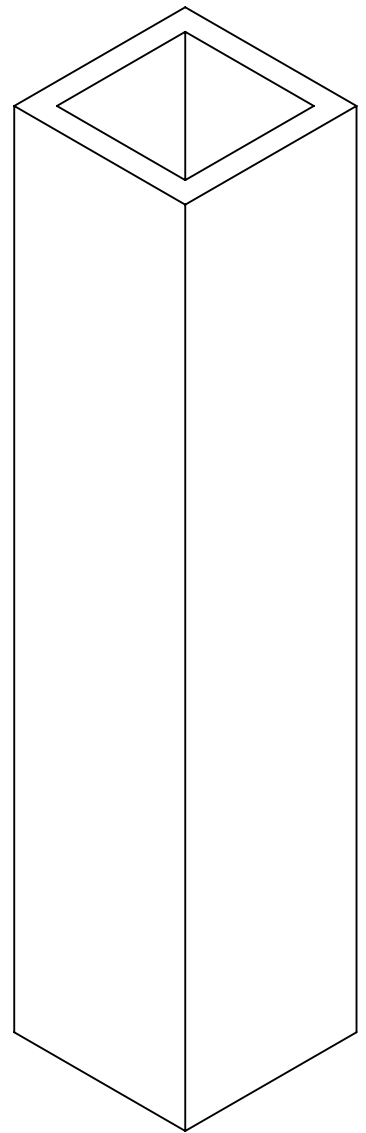
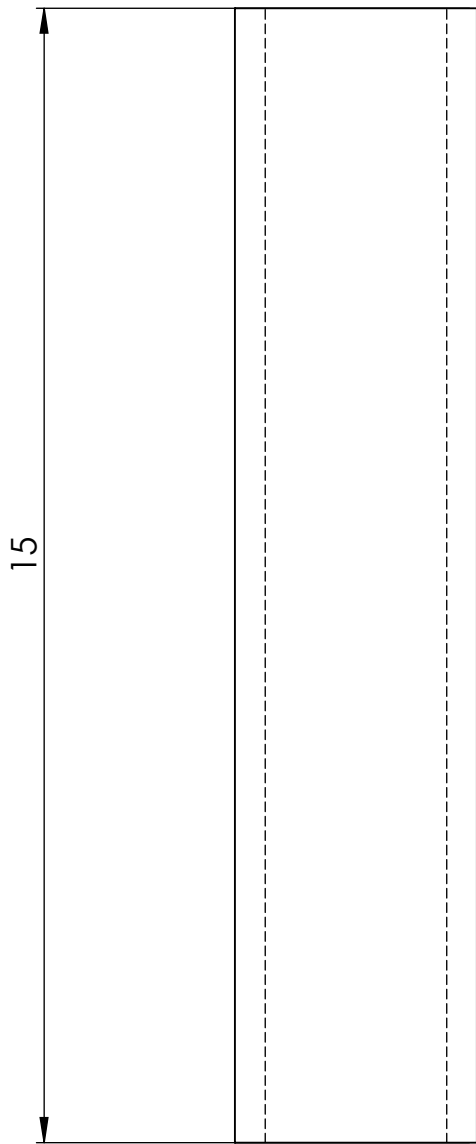
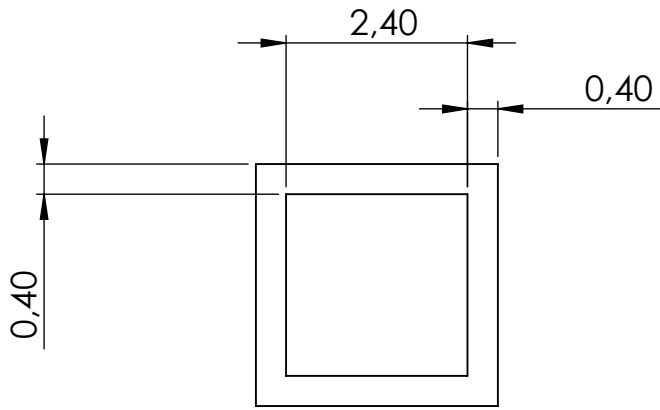
UNLESS OTHERWISE SPECIFIED: DIMENSIONS ARE IN MILLIMETERS

NAME		MATERIAL:	PLA
DRAWN	Sander Suurpere		
CHK'D	Madis Kiisk		

TITLE: **SiPM rear support**

SCALE: 1:1

SHEET 1 OF 1



A

UNLESS OTHERWISE SPECIFIED: DIMENSIONS ARE IN MILLIMETERS

	NAME		
DRAWN	Sander Suurpere	MATERIAL:	PLA
CHK'D	Madis Kiisk		

TITLE:
Fibre bundle collar

SCALE:10:1

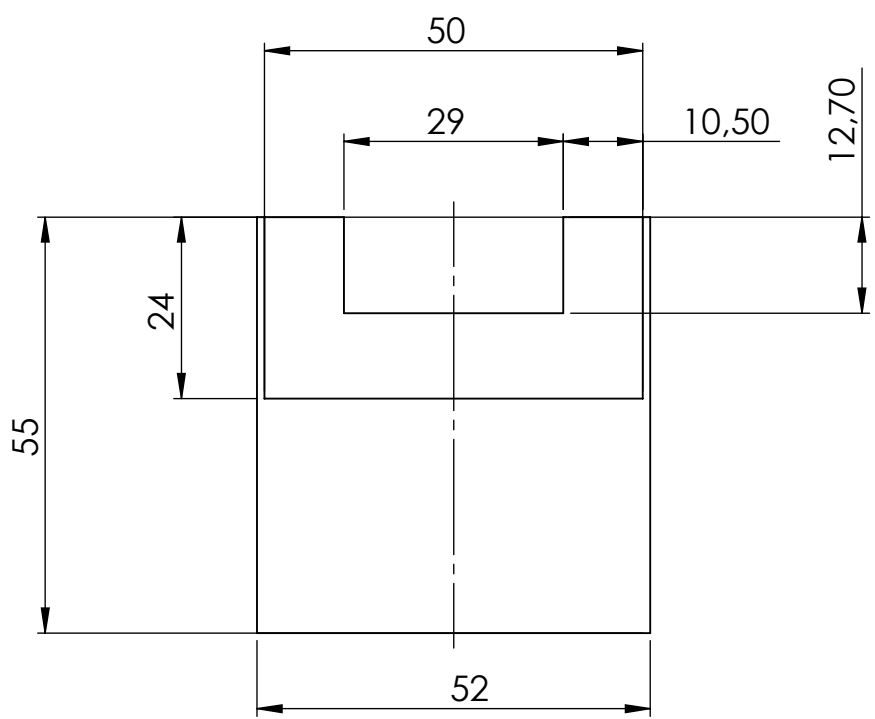
SHEET 1 OF 1

A

4 3 2 1

F

F

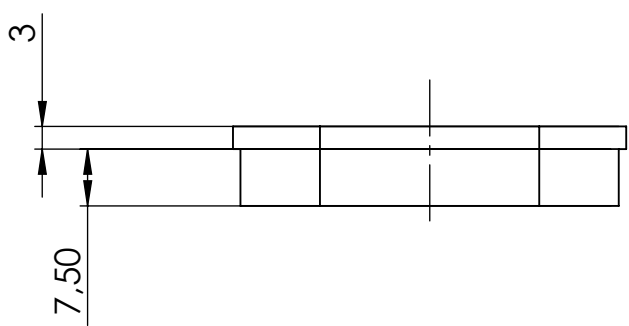


E

E

D

D

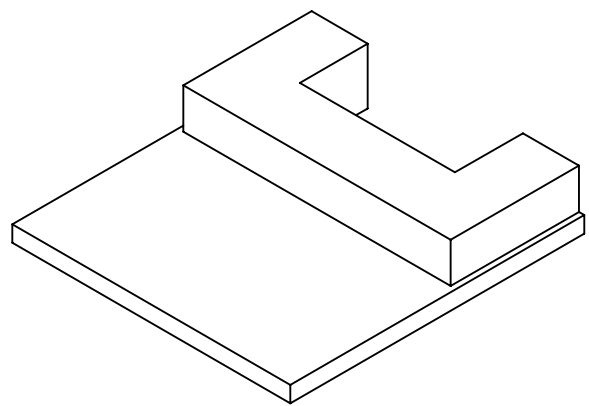


C

C

B

B



A

A

UNLESS OTHERWISE SPECIFIED: DIMENSIONS ARE IN MILLIMETERS

TITLE: Polishing support

NAME

MATERIAL: PLA

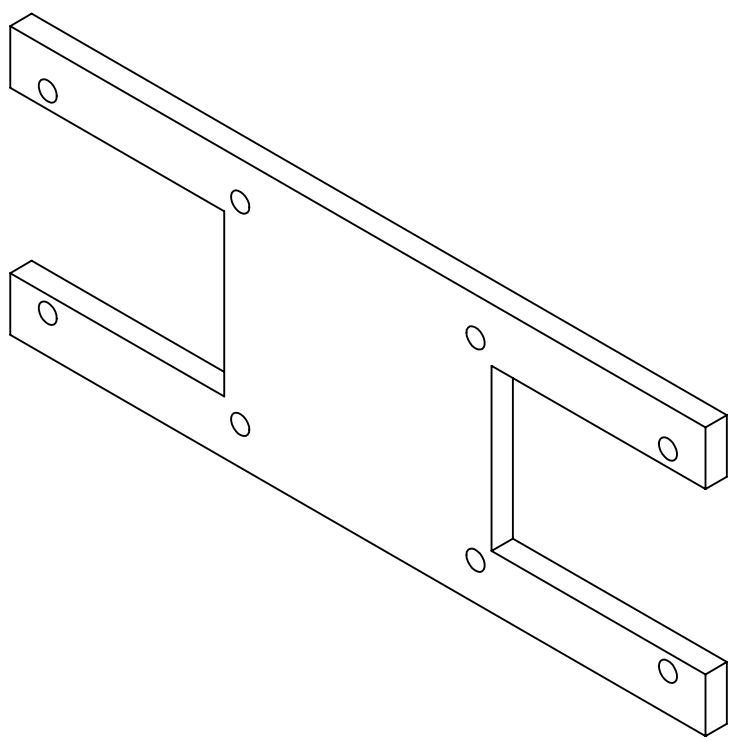
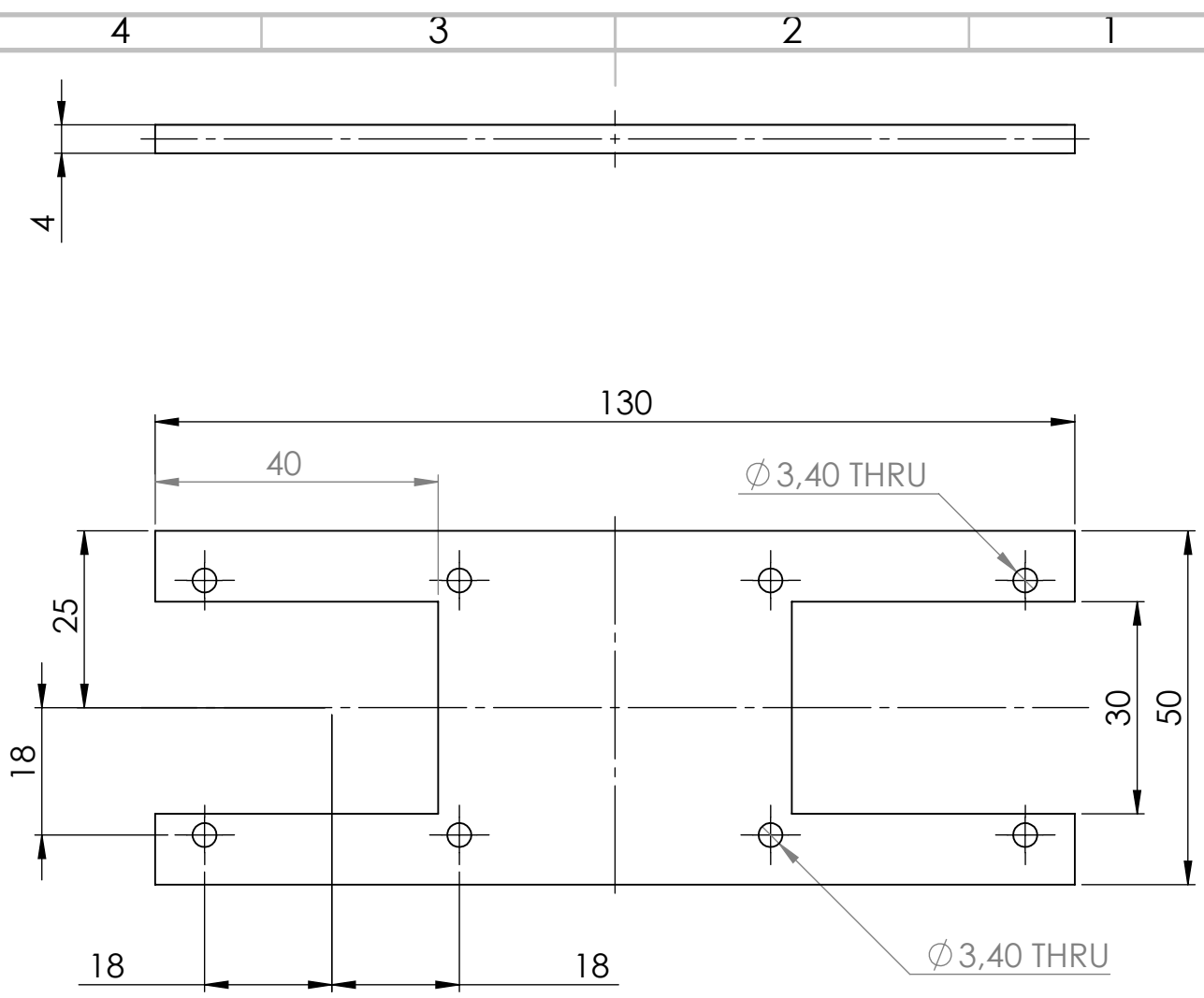
DRAWN Sander Suurpere

SCALE: 1:1

SHEET 1 OF 1

CHK'D Madis Kiisk

4 3 2 1



UNLESS OTHERWISE SPECIFIED: DIMENSIONS ARE IN MILLIMETERS

NAME		MATERIAL:	PLA
DRAWN	Sander Suurpere		
CHK'D	Madis Kiisk		

TITLE: **Gluing support**

SCALE: 1:1

SHEET 1 OF 1

Non-exclusive licence to reproduce thesis and make thesis public

I, Sander Suurpere,

1. herewith grant the University of Tartu a free permit (non-exclusive licence) to reproduce, for the purpose of preservation, including for adding to the DSpace digital archives until the expiry of the term of copyright,

Design and implementation of a cosmic ray muon detector,

supervised by Madis Kiisk, PhD and Anzori Georgadze, PhD.

2. I grant the University of Tartu a permit to make the work specified in p. 1 available to the public via the web environment of the University of Tartu, including via the DSpace digital archives, under the Creative Commons licence CC BY NC ND 3.0, which allows, by giving appropriate credit to the author, to reproduce, distribute the work and communicate it to the public, and prohibits the creation of derivative works and any commercial use of the work until the expiry of the term of copyright.
3. I am aware of the fact that the author retains the rights specified in p. 1 and 2.
4. I certify that granting the non-exclusive licence does not infringe other persons' intellectual property rights or rights arising from the personal data protection legislation.

Sander Suurpere

20/05/2019